Frustration-induced complexity in order-disorder transitions of the J_1-J_2-J_3 Ising model on the square lattice

Rodolfo Subert [1,*] and Bela M. Mulder [1,2]

[1] *Institute AMOLF, Science Park 104, 1098XG Amsterdam, The Netherlands*

[2] *Institute for Theoretical Physics, Utrecht University, Princetonplein 5, 3584 CC Utrecht, The Netherlands*

(Received 17 December 2021; revised 4 April 2022; accepted 2 June 2022; published 7 July 2022)

We revisit the field-free Ising model on a square lattice with up to third-neighbor (NNNN) interactions, also known as the J_1-J_2-J_3 model, in the mean-field approximation. Using a systematic enumeration procedure, we show that the region of phase space in which the high-temperature disordered phase is stable against all modes representing periodic magnetization patterns up to a given size is a convex polytope that can be obtained by solving a standard vertex enumeration problem. Each face of this polytope corresponds to a set of coupling constants for which a single set of modes, equivalent up to a symmetry of the lattice, bifurcates from the disordered solution. While the structure of this polytope is simple in the half-space $J_3 > 0$, where the NNNN interaction is ferromagnetic, it becomes increasingly complex in the half-space $J_3 < 0$, where the antiferromagnetic NNNN interaction induces strong frustration. We then pass to the limit $N \to \infty$ giving a closed-form description of the order-disorder surface in the thermodynamic limit, which shows that for $J_3 < 0$, the emergent ordered phases will have a "devil's surface"-like mode structure. Finally, using Monte Carlo simulations, we show that for small periodic systems, the mean-field analysis correctly predicts the dominant modes of the ordered phases that develop for coupling constants associated with the centroid of the faces of the disorder polytope.

DOI: 10.1103/PhysRevE.106.014105

I. INTRODUCTION

A few years back, Jacobs *et al.* [1], inspired by the advances in creating nanoparticles that interact highly specifically by leveraging the extreme selectivity of the base-pairing interaction in DNA, introduced the notion of self-assembling systems with "addressable complexity," i.e., the creation of regular structures in which one has full control over the spatial arrangement of different particle types. Stylized prototypes of such systems are multicomponent lattice gases with isotropic interactions in which one is free to choose the strength, sign, selectivity, and range(s) of the interparticle interactions.

Arguably the simplest system of this type is the equal mole fraction binary lattice gas, which can be mapped onto the field-free (i.e., equal chemical potential) Ising model. If only nearest-neighbor (NN) interactions with coupling constant J_1 are taken into account, the results strongly depend on the underlying lattice structure. On the triangular lattice, when $J_1 > 0$, we obtain a homogeneous ferromagnetic low-temperature phase (F), corresponding to a complete demixing of the particles, while for $J_1 < 0$, no long-range order develops and the system is caught in a finite-entropy ground state [2]. The square lattice, however, is bipartite and hence not frustrated by a $J_1 < 0$ coupling, and exhibits a regular antiferromagnetic (AF) checkerboard phase at low temperatures.

Thus, if one wishes to observe more complex ordering patterns on the square lattice, longer-range interactions are required, and specifically those that introduce frustration, effectively preempting the period-2 repeat of the AF state. Hence, starting in the 1970s, a long line of authors has studied the so-called frustrated Ising models obtained by introducing antiferromagnetic ($J_2 < 0$) next-nearest-neighbor (NNN) interactions on the square lattice. These additional interactions were either isotropic [3–9], with more recent work appearing in the past decade or so [10–14], or anisotropic, as in the case of the highly influential anisotropic next-nearest neighbor ising (ANNNI) model (for a comprehensive review, see [15]), which, due to its quasi-one-dimensional nature, allowed for a far more detailed analysis of its properties. As this type of interaction penalizes equal spins across the diagonal of the square unit cell, it frustrates the NN interactions independently of their sign.

However, increasing the range of interactions even further allows the degree of frustration to also be increased. Indeed, very general arguments suggest that in order to obtain the maximum complexity periodic patterns on a given lattice structure, all symmetries implied by the point group of the lattice must be suppressed by the interactions [16]. For the square lattice, this implies that next-next-nearest-neighbor couplings (NNNN) also need to be taken into account, as shown in Fig. 1. Clearly, an antiferromagnetic NNNN interaction ($J_3 < 0$) adds yet another level of frustration as it potentially frustrates *both* the NN and NNN bonds independently of the sign of their interaction. In fact, this latter extension was already actively studied a couple of decades ago, purely for its theoretical interest [8,17,18]. Strikingly, interest in this NNNN model, also known as the J_1-J_2-J_3 model, was revived in the past decade with a few theoretical studies

*Current address: Debye Institute for Nanomaterials Sciences, Utrecht University, Princetonplein 5, 3584 CC Utrecht, The Netherlands.

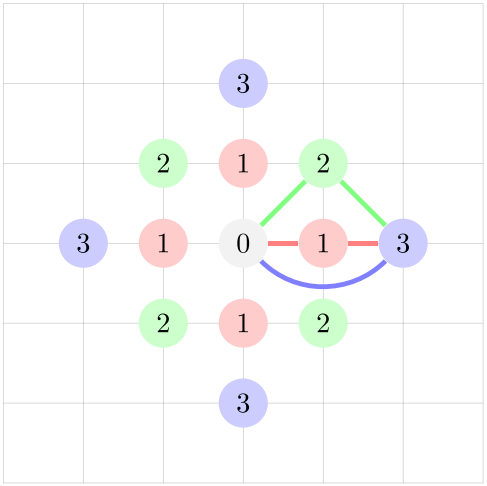

FIG. 1. The interaction neighborhoods of the origin site (0: gray site) in the range-3 Ising model on the square lattice. N_1: red sites; N_2: green sites; N_3: blue sites. An antiferromagnetic NNNN bond (blue line) between two sites frustrates the spin arrangement both along the shortest NN paths (red lines) and NNN paths (green lines) that connect them.

appearing [19,20], as well as a significant paper showing that a model with up to third-neighbor coupling is actually relevant to understanding the magnetic origin of high-T_c superconductivity in a class of iron chalcogenides [21].

Reviewing these works, however, reveals that we are far from having a complete picture of the phase behavior of these systems. Most of the effort was devoted to understanding the structure of the ground states, using either the method of inequalities introduced by Kanamori [22] or direct enumeration. These analyses are, however, all limited by implicit or explicit assumptions on the size of the considered repeating patterns. Characteristically, Landau and Binder [8] remark "Since the phase diagram is expected to be very complicated ("devil's staircase" of phases), no attempt to include these phases has been made." Where the behavior at finite temperature is concerned, the main tool has been Monte Carlo simulations, but again the attention was mostly devoted to the nature of the transitions towards certain specific states or to the behavior in response to external fields.

Driven by the question to what extent one can "design" specific magnetization patterns on the square lattice, our aim here is to provide a fresh perspective on the phase behavior of the field-free NNNN model in a way that systematically allows the consideration of phases of increasing complexity. We do this in the framework of mean-field theory, which allows us to exactly formulate the criteria if and when the high-temperature disordered phase becomes unstable to magnetization modes belonging to periodicities with increasing unit cell size N. This analysis reveals that the region in phase space where the disordered phase is stable is a convex polytope whose complexity increases as we increase N. Each of the faces of this polytope defines the values of the coupling constants for which a specific equivalence class of magnetization modes is spontaneously excited. We probe the structure of this polytope as a function of the unit cell size of the periodicities included, which provides a fingerprint of the complexity of the predicted phase space. On the basis of this analysis, we are able to analytically pass to the limit $N \to \infty$ to give a closed-form description of the order-disorder surface in the thermodynamic limit. This shows that in the strongly frustrated region of phase space $J_3 < 0$, the mean-field theory predicts a "devil's surface"-like structure for the modes developing from the disordered phase, in which in an arbitrarily small neighborhood of any set of coupling parameters, one can find phases of arbitrary spatial complexity becoming stable.

While the mean-field results are quantitatively, at best, a strong approximation of the true phase boundaries, the predictions regarding the possible symmetry-breaking patterns, however, are potentially more robust. We explore this latter premise by performing Monte Carlo (MC) simulations with the appropriate finite periodic boundary conditions along rays in phase space, corresponding to decreasing temperature at fixed coupling constants, that pass through the centers of the predicted mode instability faces. These show that the mean-field analysis consistently correctly predicts the dominant mode first appearing in the ordered region in the cases considered.

The structure of the paper is as follows: In Sec. II, we set up the model. The mean-field treatment is discussed in Sec. III. The stability analysis of the high-temperature disordered phase is presented in Sec. IV, which introduces our main object of interest, the disorder polytope and its surface. In Sec. V, we first discuss the phenomenology of the disorder polytope for finite N (Sec. V A) and then take the limit $N \to \infty$ (Sec. V B), leading to our major result, the prediction of the full order-disorder surface. Finally, in Sec. VI, we show using Monte Carlo simulations that for finite N, implemented through periodic boundary conditions, the mean-field analysis correctly predicts the bifurcating modes. After the discussion given in Sec. VII, Appendices A–F gather some more detailed technical results needed in the main text.

II. MODEL

We consider the two-dimensional square lattice, $\mathrm{L} = \{\mathrm{z} = (z^1, z^2) | z^1, z^2 \in \mathbb{Z}\}$. Throughout, we will use lowercase roman letters to denote the sites of the lattice, and uppercase roman letters to denote sets of sites. We also make use of the fact that the square lattice forms a group under vector addition, which is generated by the basis vectors $\mathrm{e}_1 = (1, 0)$ and $\mathrm{e}_2 = (0, 1)$ and can be equipped with an inner product $\langle \mathrm{z}, \mathrm{z}' \rangle = z^1 z^{1\prime} + z^2 z^{2\prime}$. The sites of the lattice are occupied by Ising spins, $\sigma_\mathrm{z} \in \{-1, 1\}$. To denote a spin configuration on a set of sites C, we use the notation σ_C. We define the *range* $r(\mathrm{z}, \mathrm{z}')$ between two distinct sites as the index of the Euclidean distance $|\mathrm{z} - \mathrm{z}'|$ in the ordered list of distances between sites of the lattice, with $r = 1$ denoting nearest neighbors ($|\mathrm{z} - \mathrm{z}'| = 1$), $r = 2$ next-nearest neighbors ($|\mathrm{z} - \mathrm{z}'| = \sqrt{2}$), $r = 3$ next-next-nearest neighbors ($|\mathrm{z} - \mathrm{z}'| = 2$), and so on. We focus on the field-free range-3 Ising model, defined by the Hamiltonian

$$\mathcal{H}(\sigma_\mathrm{L}) = -J_1 \sum_{r(\mathrm{z},\mathrm{z}')=1} \sigma_\mathrm{z}\sigma_{\mathrm{z}'} - J_2 \sum_{r(\mathrm{z},\mathrm{z}')=2} \sigma_\mathrm{z}\sigma_{\mathrm{z}'} - J_3 \sum_{r(\mathrm{z},\mathrm{z}')=3} \sigma_\mathrm{z}\sigma_{\mathrm{z}'}, \tag{1}$$

where the minus sign in front of the *coupling constants* J_1, J_2, and J_3 is conventional. Further on, we will make regular use of the the range-r neighborhoods of the origin,

$$\mathrm{N}_1 = \{\mathrm{e}_1, -\mathrm{e}_1, \mathrm{e}_2, -\mathrm{e}_2\}, \tag{2}$$

$$\mathrm{N}_2 = \{\mathrm{e}_1 + \mathrm{e}_2, -\mathrm{e}_1 - \mathrm{e}_2, \mathrm{e}_1 - \mathrm{e}_2, -\mathrm{e}_1 + \mathrm{e}_2\}, \tag{3}$$

$$\mathrm{N}_3 = \{2\mathrm{e}_1, -2\mathrm{e}_1, 2\mathrm{e}_2, -2\mathrm{e}_2\}, \tag{4}$$

which we show in Fig. 1.

III. MEAN-FIELD THEORY

Our approach to understanding the phase behavior of the model (1) is through mean-field theory (MFT). Although MFT is a drastic approximation, and *a fortiori* so in lower dimensions, it nevertheless generically is a good guide into the possible phases a system can display, as these are, to a large extent, determined by universal symmetry relations (see, e.g., [23,24]). MFT is typically formulated as a set of self-consistent equations for the single-site spin probabilities,

$$P_{\mathrm{z}}(\sigma_{\mathrm{z}}) = \frac{e^{-\beta V_{\mathrm{z}}(\sigma_{\mathrm{z}})}}{\sum_{\sigma_{\mathrm{z}}} e^{-\beta V_{\mathrm{z}}(\sigma_{\mathrm{z}})}}, \tag{5}$$

where $\beta = 1/k_B T$ is the inverse temperature and the effective mean field $V_{\mathrm{z}}(\sigma_{\mathrm{z}})$ itself depends on the spin probabilities on all the sites with which the spin σ_{z} interacts,

$$\begin{aligned} V_{\mathrm{z}}(\sigma_{\mathrm{z}}) = -\sigma_{\mathrm{z}} \Bigg\{ & J_1 \sum_{\mathrm{n}_1 \in \mathrm{N}_1} \sum_{\sigma_{\mathrm{z}+\mathrm{n}_1}} \sigma_{\mathrm{z}+\mathrm{n}_1} P_{\mathrm{z}+\mathrm{n}_1}(\sigma_{\mathrm{z}+\mathrm{n}_1}) \\ & + J_2 \sum_{\mathrm{n}_2 \in \mathrm{N}_2} \sum_{\sigma_{\mathrm{z}+\mathrm{n}_2}} \sigma_{\mathrm{z}+\mathrm{n}_2} P_{\mathrm{z}+\mathrm{n}_2}(\sigma_{\mathrm{z}+\mathrm{n}_2}) \\ & + J_3 \sum_{\mathrm{n}_3 \in \mathrm{N}_3} \sum_{\sigma_{\mathrm{z}+\mathrm{n}_2}} \sigma_{\mathrm{z}+\mathrm{n}_3} P_{\mathrm{z}+\mathrm{n}_3}(\sigma_{\mathrm{z}+\mathrm{n}_3}) \Bigg\}. \end{aligned} \tag{6}$$

The averages over the spin values in this expression can all be succinctly summarized using the definition of the site magnetization,

$$m(\mathrm{z}) = \sum_{\sigma_{\mathrm{z}}} \sigma_{\mathrm{z}} P_{\mathrm{z}}(\sigma_{\mathrm{z}}), \tag{7}$$

which allows us to reformulate (5) as

$$m(\mathrm{z}) = \frac{\sum_{\sigma_{\mathrm{z}}} \sigma_{\mathrm{z}} e^{-W_{\mathrm{z}}(\sigma_{\mathrm{z}})}}{\sum_{\sigma_{\mathrm{z}}} e^{-W_{\mathrm{z}}(\sigma_{\mathrm{z}})}}, \tag{8}$$

with

$$\begin{aligned} W_{\mathrm{z}}(\sigma_{\mathrm{z}}) = -\sigma_{\mathrm{z}} \Bigg\{ & K_1 \sum_{\mathrm{n}_1 \in \mathrm{N}_1} m(\mathrm{z}+\mathrm{n}_1) + K_2 \sum_{\mathrm{n}_2 \in \mathrm{N}_2} m(\mathrm{z}+\mathrm{n}_2) \\ & + K_3 \sum_{\mathrm{n}_3 \in \mathrm{N}_3} m(\mathrm{z}+\mathrm{n}_3) \Bigg\}, \end{aligned} \tag{9}$$

where we have absorbed the common positive prefactor β into the now dimensionless coupling constants $K_r = \beta J_r$.

In anticipation of the further developments below, it will turn out to be convenient to consider the triplets of possible values of the coupling constants K_1, K_2, and K_3 as a linear vector space, whose elements we will denote by bold symbols, viz., $\mathbf{K} = (K_1, K_2, K_3)$. To further compactify the notation, we also introduce summed neighborhood magnetizations,

$$M_r(\mathrm{z}) = \sum_{\mathrm{n}_r \in \mathrm{N}_r} m(\mathrm{z}+\mathrm{n}_r), \tag{10}$$

and define $\mathbf{M}(\mathrm{z}) = [M_1(\mathrm{z}), M_2(\mathrm{z}), M_3(\mathrm{z})]$, so that $W_{\mathrm{z}}(\sigma_{\mathrm{z}}) = -\sigma_{\mathrm{z}} \mathbf{K} \cdot \mathbf{M}(\mathrm{z})$, where the center dot is the Euclidean inner product. Using these definitions, we can simplify Eq. (8) to take on the familiar form

$$m(\mathrm{z}) = \tanh\left[\mathbf{K} \cdot \mathbf{M}(\mathrm{z})\right], \tag{11}$$

which constitutes an (infinite) set of coupled nonlinear self-consistency equations for the magnetizations $\{m(\mathrm{z})\}_{\mathrm{z}\in\mathrm{L}}$.

IV. STABILITY ANALYSIS OF THE DISORDERED PHASE

A. Bifurcation equation

We do not attempt to solve Eqs. (11) in all generality, but focus on understanding the phases that develop from the high-temperature disordered phase upon a temperature quench. First note that infinite temperature ($\beta = 0$) corresponds to the origin $\mathbf{K} = 0$ of the three-dimensional phase space of the model. It is easy to see that in this point, all spins are decoupled as the effective field vanishes, and we have $m(\mathrm{z}) = 0$. Moreover, by the same token, the disordered state with $m(\mathrm{z}) = 0$ for which $\mathbf{M}(\mathrm{z}) = 0$ is in fact a solution for any value of $\mathbf{K}$. We now inquire at which values of $\mathbf{K}$ Eq. (11) can support a nonzero solution. To that end we expand Eq. (11) to first order in the magnetizations, yielding

$$m(\mathrm{z}) = \mathbf{K} \cdot \mathbf{M}(\mathrm{z}). \tag{12}$$

The values of the coupling constants $\mathbf{K}$ for which this set of equations admits a nonzero solution defines the set of *order-disorder points*, in which an ordered solution to the self-consistency equation branches off from the disordered solution.

Since $\mathbf{M}(\mathrm{z})$ [cf. Eq. (10)] involves the magnetization of all sites in the interaction neighborhood of z, even in the linear approximation defining the bifurcation equation, the magnetizations of all sites remain coupled. To proceed, we therefore take the Fourier transform of (12) with respect to lattice compatible wave vectors, which generically are of the form

$$\mathrm{q} = 2\pi\left(\frac{j_1}{n_1}, \frac{j_2}{n_2}\right), \; j_i \in \mathbb{Z}, n_i \in \mathbb{N}^+, \tag{13}$$

to obtain

$$\hat{m}(\mathrm{q}) = \mathbf{K} \cdot \mathbf{F}(\mathrm{q})\, \hat{m}(\mathrm{q}), \tag{14}$$

where $\mathbf{F}(\mathrm{q}) \equiv [F_1(\mathrm{q}), F_2(\mathrm{q}), F_3(\mathrm{q})]$ is the set of Fourier transforms of the indicator functions of the neighborhood clusters defined through

$$F_r(\mathrm{q}) = \sum_{\mathrm{n}_r \in \mathrm{N}_r} e^{-i\langle \mathrm{n}_r, \mathrm{q}\rangle}. \tag{15}$$

For the range-3 model on the square lattice, the relevant lattice neighborhood transforms are

$$F_1(\mathrm{q}) = 2\cos q_1 + 2\cos q_2, \tag{16}$$

$$F_2(\mathrm{q}) = 2\cos(q_1 - q_2) + 2\cos(q_1 + q_2), \tag{17}$$

$$F_3(\mathrm{q}) = 2\cos 2q_1 + 2\cos 2q_2. \tag{18}$$

An important property of these functions is that they are invariant with respect to the point symmetry group of the lattice—here, the dihedral group $\mathfrak{D}_4$ is the symmetry group of a square. Let G be the real unitary two-dimensional (2D) matrix representation of $\mathfrak{D}_4$; then, for any element $\mathrm{g} \in \mathrm{G}$,

$$\begin{aligned} F_r(\mathrm{gq}) &= \sum_{\mathrm{n}_r \in \mathrm{N}_r} e^{-i\langle \mathrm{n}_r, \mathrm{gq}\rangle} = \sum_{\mathrm{gn}_r \in \mathrm{N}_r} e^{-i\langle \mathrm{gn}_r, \mathrm{gq}\rangle} \\ &= \sum_{\mathrm{n}_r \in \mathrm{N}_r} e^{-i\langle \mathrm{n}_r, \mathrm{q}\rangle} = F_r(\mathrm{q}), \end{aligned} \tag{19}$$

where we have used the fact that g simply permutes the sites of the lattice neighborhoods N_r. This implies that instead of individual modes, it suffices to consider the equivalence classes of modes defined by the orbits $\mathrm{Gq} = \{\mathrm{gq}|\mathrm{g} \in \mathrm{G}\}$. In passing, we also note that (14) is in fact readily generalized to other lattices and models with longer-range pair interactions, as the lattice structure enters only through the functions $\mathbf{F}(\mathrm{q})$, and increasing the range of the pair interactions simply requires increasing the dimensionality of the phase space spanned by the coupling-constant vectors $\mathbf{K}$.

As Eq. (14) shows, close to a bifurcation, all magnetization modes are decoupled. Also, it is clear that the loci in phase space at which the state with zero magnetization becomes unstable to the mode q lie on the plane $L_\mathrm{q} = \{\mathbf{K}|\mathbf{K}\cdot\mathbf{F}(\mathrm{q}) = 1\}$. Since at infinite temperature, where $\mathbf{K} = \mathbf{0}$, the system is surely disordered, we infer that the disordered phase is stable against this mode in the half space containing the origin bounded by L_q, i.e.,

$$H_\mathrm{q} = \{\mathbf{K}|\mathbf{K}\cdot\mathbf{F}(\mathrm{q}) < 1\}. \tag{20}$$

B. Enumerating the lattice modes

The problem we now face, however, is that there are, in principle, an infinite number of modes in the Brillouin zone of the square lattice $\widehat{\mathcal{U}}_\infty \equiv [0, 2\pi) \times [0, 2\pi) \subset \mathbb{R}^2$ to consider. In order to tackle this problem, we choose to systematically enumerate the potential modes, ordering them by a natural measure of the "size" of the periodicity they represent. Each periodically repeating pattern on the lattice L is characterized by two basis vectors $\mathrm{p}_1 = (p_1^1, p_1^2)$, $\mathrm{p}_2 = (p_2^1, p_2^2) \in \mathbb{Z}^2$ conveniently presented in matrix form,

$$\mathrm{P} = \begin{pmatrix} p_1^1 & p_1^2 \\ p_2^1 & p_2^2 \end{pmatrix}, \tag{21}$$

where we choose the order of p_1 and p_2 such that $\det \mathrm{P} = N > 0$. It is easy to see that N is just the number of sites in the unit cell $\mathcal{U}_\mathrm{P}$ of the periodic pattern. We call it the *index* of the periodicity, following the mathematical nomenclature that associates it with the size of the quotient group L/P when P is interpreted as a subgroup of L [25]. In Appendix A,

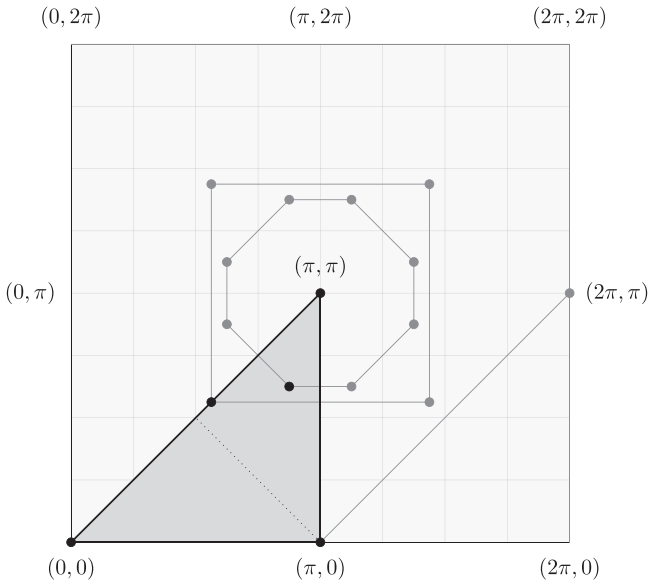

FIG. 2. Geometry of the irreducible Brillouin zone $\widehat{\mathfrak{U}}_\infty = \widehat{\mathcal{U}}_\infty/G$, depicted as the shaded triangle. Multiplicities: $M = 1$: the points (0,0) and (π, π); $M = 2$: the point $(\pi, 0)$; $M = 4$: all boundary points, excluding the vertices; $M = 8$: all interior points. Also shown are three representative orbits in the embedding space, $\widehat{\mathcal{U}}_\infty = [0, 2\pi) \times [0, 2\pi)$. The dotted antidiagonal is the unique line of the mirror symmetry of $\widehat{\mathfrak{U}}_\infty$.

we review the construction of periodic patterns on L, their corresponding discrete sets of Brillouin vectors $\widehat{\mathcal{U}}_\mathrm{P}$, and their enumeration. An important result is that the structure of the set,

$$\widehat{\mathcal{U}}_N = \bigcup_{\{\mathrm{P}||\widehat{\mathcal{U}}_\mathrm{P}|=N\}} \widehat{\mathcal{U}}_\mathrm{P} = \left\{ \mathrm{q} = \frac{2\pi}{N}(l_1, l_2) | 0 \leqslant l_1, l_2 < N \right\}, \tag{22}$$

which includes the wave vectors of all patterns of index N, is simply a square array and equal to the set of Brillouin vectors of the square $N \times N$ periodicity $\mathrm{P}_{\square N} = \mathrm{diag}(N, N)$. For any lattice mode q, we can define its *complexity* as the smallest square periodicity to which it belongs [26]. If

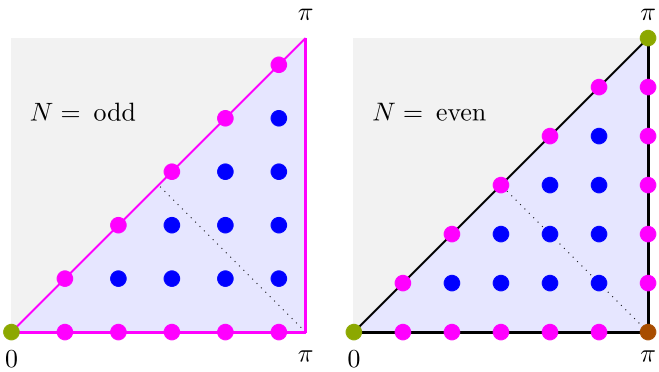

FIG. 3. Modes in $\widehat{\mathfrak{U}}_N$ for $N =$ odd and $N =$ even. Multiplicities are color coded: $M = 1$: green; $M = 2$: brown; $M = 4$: purple; $M = 8$: blue. $\widehat{\mathfrak{U}}_N$ is mirror symmetric with respect to the dotted antidiagonal for even N.

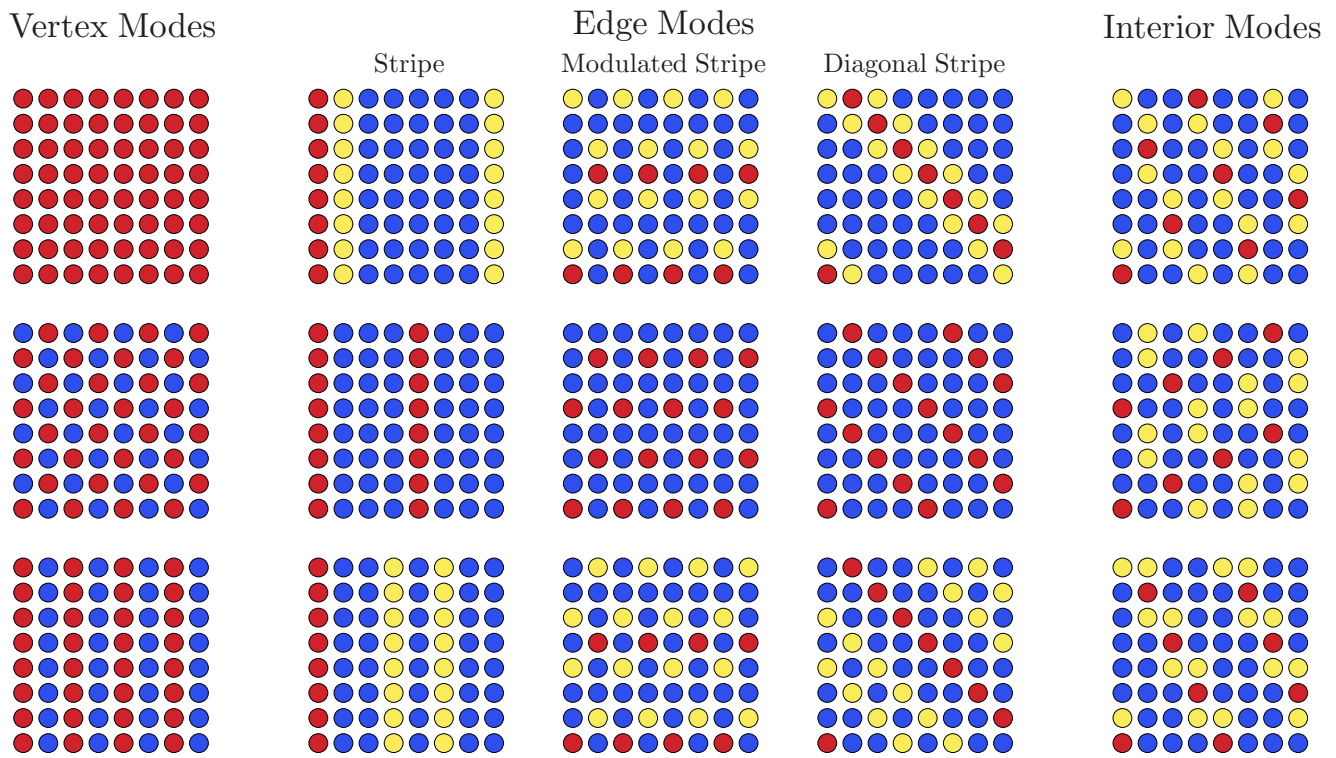

FIG. 4. Visualization of ordering patterns for different modes. Leftmost column: The major modes with from top to bottom, $\mathfrak{q}^F = (0,0)$, $\mathfrak{q}^{AF} = (\pi,\pi)$ and $\mathfrak{q}^{AS} = (\pi,0)$. Middle three columns: Multiplicity $M = 4$ edge modes, with in the top row striped modes $\mathfrak{q} = \frac{\pi}{6}(1,0)$, $\mathfrak{q} = \frac{\pi}{6}(3,0)$ and $\mathfrak{q} = \frac{\pi}{6}(5,0)$, in the middle row modulated stripe modes $\mathfrak{q} = \frac{\pi}{6}(6,1)$, $\mathfrak{q} = \frac{\pi}{6}(6,3)$ and $\mathfrak{q} = \frac{\pi}{6}(6,5)$, and in the bottom row diagonal stripe modes $\mathfrak{q} = \frac{\pi}{6}(1,1)$, $\mathfrak{q} = \frac{\pi}{6}(3,3)$ and $\mathfrak{q} = \frac{\pi}{6}(5,5)$. Rightmost column: Multiplicity $M = 8$ interior modes with, from top to bottom $\mathfrak{q} = \frac{\pi}{6}(2,1)$, $\mathfrak{q} = \frac{\pi}{6}(3,2)$ and $\mathfrak{q} = \frac{\pi}{6}(5,3)$.

$\mathrm{q} = (2\pi n_1/d_1, 2\pi n_2/d_2)$ with n_i and d_i relatively prime, then the complexity is simply given by $C(\mathrm{q}) = \mathrm{lcm}(d_1, d_2)$.

In view of the invariance (19) of the neighborhood transforms $F_r(\mathrm{q})$, however, the proper degrees of freedom for the mode analysis are the elements of the orbit space,

$$\widehat{\mathfrak{U}}_\infty \equiv \widehat{\mathcal{U}}_\infty / G = \{G\mathrm{q} | \mathrm{q} \in \widehat{\mathcal{U}}_\infty\}, \tag{23}$$

where $G = \mathfrak{D}_4$ is the point group of the lattice. The set $\widehat{\mathfrak{U}}_N$ is commonly called the irreducible Brillouin zone (IBZ). Throughout, we will use a gothic-style font to denote elements of the IBZ, e.g., $\mathfrak{q}$. Different $\mathrm{q} \in \widehat{\mathcal{U}}_\infty$ behave differently under the action of the point-symmetry group G, depending on their location within $\widehat{\mathcal{U}}_\infty$. To each irreducible mode $\mathfrak{q}$, we can associate a *multiplicity* $M(\mathfrak{q}) = |G\mathfrak{q}|$, the length of the orbit under the action of G to which it belongs, which will play an important role in the further analysis. According to the fundamental theorem of group actions, the possible multiplicities under the group $\mathfrak{D}_4$ are given by the four divisors $\{1, 2, 4, 8\}$ of its order $|\mathfrak{D}_4| = 8$. The structure of the IBZ, including the multiplicities associated with the orbits of some of its elements, is illustrated in Fig. 2.

For finite N, we are interested in the discrete set of irreducible modes, $\widehat{\mathfrak{U}}_N = \widehat{U}_N \cap \widehat{\mathfrak{U}}_\infty$. The structure of these sets depends on the properties of N and is illustrated in Fig. 3. The number of modes in $\widehat{\mathfrak{U}}_N$ is discussed in Appendix B.

The nature of the magnetization patterns corresponding to the irreducible modes depends on their multiplicity and location within $\widehat{\mathfrak{U}}_\infty$. We distinguish three classes. First are the modes associated with the vertices of $\widehat{\mathfrak{U}}_\infty$, which we will call *major* modes. These are $\mathfrak{q}^F = (0,0)$ ($M = 1$), $\mathfrak{q}^{AF} = (\pi,\pi)$ ($M = 1$), and $\mathfrak{q}^{AS} = (\pi,0)$ ($M = 2$). These are visualized in Fig. 4 and correspond to *ferromagnetic* (F), *antiferromagnetic* (AF), and *alternating stripe* (AS) ordering patterns, respectively. In this and the following visualizations, the index of the periodicity is $N = 12$ and the amplitude of the modes is normalized by setting the value of the origin site to 1, represented by the color red. The other amplitude values are then shown on a temperature-type scale, with dark blue corresponding to the minimum value -1. Next are the $M = 4$ *edge modes* located on the boundary of $\widehat{\mathfrak{U}}_\infty$. Here we distinguish the modes on the horizontal edge $\mathfrak{q}^S(\lambda) = (\lambda\pi, 0)$, the vertical edge $\mathfrak{q}^{MS}(\lambda) = (\pi, \lambda\pi)$, and the hypotenuse $\mathfrak{q}^{DS}(\lambda) = (\lambda\pi, \lambda\pi)$, where, in all cases, $\lambda \in [0,1]$. We visualize these in Fig. 4, showing that these correspond to *stripe* (S), *modulated stripe* (MS), and *diagonal stripe* (DS) magnetization patterns, respectively. The wavelength of these patterns obviously depends on N. The final class is formed by the $M = 8$ modes from the interior of the IBZ. We visualize some of these in Fig. 4, noting that these are lower-symmetry patterns that are hard to characterize generically.

C. The disordered region and the order-disorder surface

We now define our main object of interest, the region D_N around the origin in phase space in which the disordered solution is stable against all modes in $\widehat{\mathfrak{U}}_N$. This region is formed by

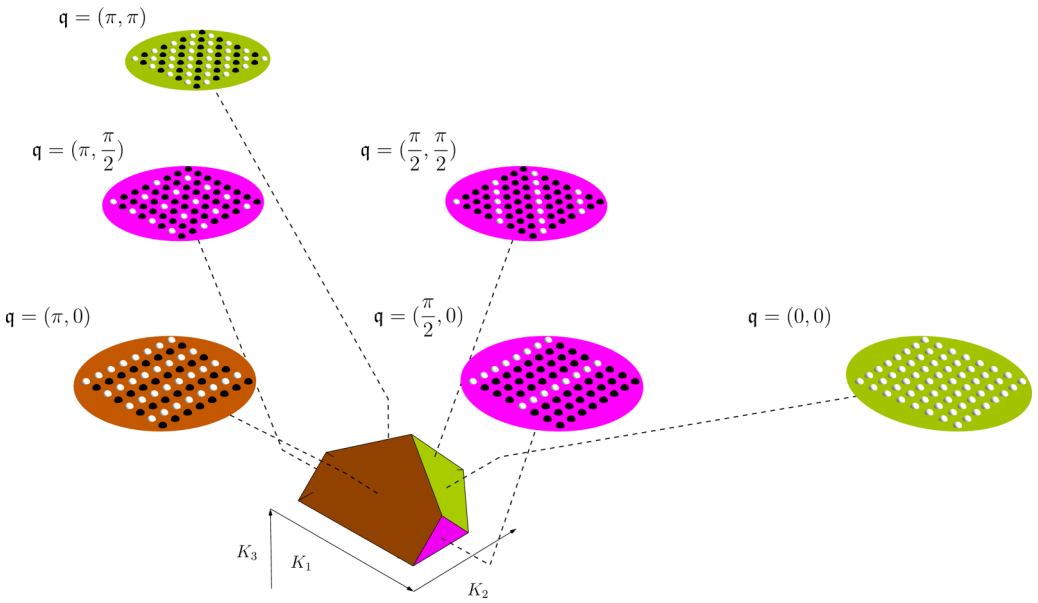

FIG. 5. The order-disorder surface of the NNNN-Ising model for modes with periodic unit cell with size $N = 4$ in the space of coupling dimensionless coupling constants (K_1, K_2, K_3). Each of the faces of this polytope is labeled by the wave vector $\mathfrak{q} = 2\pi(\frac{i}{4}, \frac{j}{4})$ of the mode in the irreducible Brillouin zone that becomes unstable at this face, and the corresponding periodic pattern of magnetizations is visualized.

the intersection of all the half spaces of the type $H_\mathfrak{q}$ defined in Eq. (20) in which the system is stable against the irreducible mode $\mathfrak{q}$, i.e.,

$$D_N = \bigcap_{\mathfrak{q} \in \widehat{\Omega}_N} H_\mathfrak{q}. \tag{24}$$

Generically, the intersection of a finite number of half spaces is a so-called convex *polytope*, a bounded polyhedron [27]. Our main goal here is to understand the structure of these *disorder polytopes* and their behavior as a function of N. The surface of the disorder polytopes is the locus in phase space where the disordered high-temperature solution becomes unstable, which we will call the *order-disorder surface*. Note that not all modes in $\widehat{\Omega}_N$ necessarily contribute a face to D_N: These "faceless" modes are preempted by other modes whose instability surface lies closer to the origin. The problem of determining the structure of a polytope from the set of defining half spaces is known as the *vertex enumeration problem*. Intriguingly, the computational complexity of the vertex enumeration problem in its most general form is as yet undecided [28]. However, several well-developed algorithms exist that are both polynomial in time and memory when the polytopes are known to be bounded [29].

In Fig. 5, we illustrate the relationship between the faces of order-disorder surface, the boundary of the polytope D_4, the modes $\mathfrak{q} \in \widehat{\Omega}_N$ in the IBZ which become unstable at these faces, and the periodic magnetization patterns that these modes represent.

Ultimately, we are, of course, interested in the limit $N \to \infty$, where all restrictions on the periodicity of the bifurcation modes are lifted, to obtain the full domain of stability of the disordered phase, i.e.,

$$D_\infty = \lim_{N \to \infty} D_N. \tag{25}$$

We will show below how D_∞ can be fully constructed in part based on the results for finite N.

V. THE GEOMETRY OF THE ORDER-DISORDER SURFACE

A. Finite N

We first present an overview of the results on the disorder polytopes for finite N. These results were obtained using the vertex enumeration package lrs based on the algorithm developed by Avis and Fukuda [30,31], with bespoke post-processing to remove rationalization artifacts (for details, see Appendix C), and rendered with *Mathematica* [32]. As we go along, we point out a number of features that are dealt with in more detail in Appendix D.

We start off by noting that D_1, D_2, and D_3 are unbounded convex polyhedra, as they lack the requisite number of constraints to create a bounded domain, and we therefore do not display them. In Fig. 6, we show the disorder polytopes D_4 through D_9. Throughout, we will use a color code to indicate the multiplicity of the mode corresponding to each face of the polytope: $M = 1$: green; $M = 2$: brown; $M = 4$: purple; $M = 8$: blue. Two features immediately stand out. First, the polytopes with even N appear symmetric upon changing the sign of K_1, whereas those with odd N are clearly asymmetric in this respect. We discuss the origin of this symmetry in Appendix D 1. Second, the top of the polytope in the half space $K_3 > 0$ is bounded by just three faces, which moreover appear to be the same ones for all even N. In the even-N case, three faces are associated with the previously introduced three major modes located in the vertices of the IBZ, with the ones associated with $\mathfrak{q}^F$ and $\mathfrak{q}^{AF}$ forming a symmetric pair facing in the positive-K_2 direction, and the face associated with $\mathfrak{q}^{AS}$, itself mirror symmetric in the K_2-K_3 plane, facing in the negative-K_2 direction. The geometry of the top of the

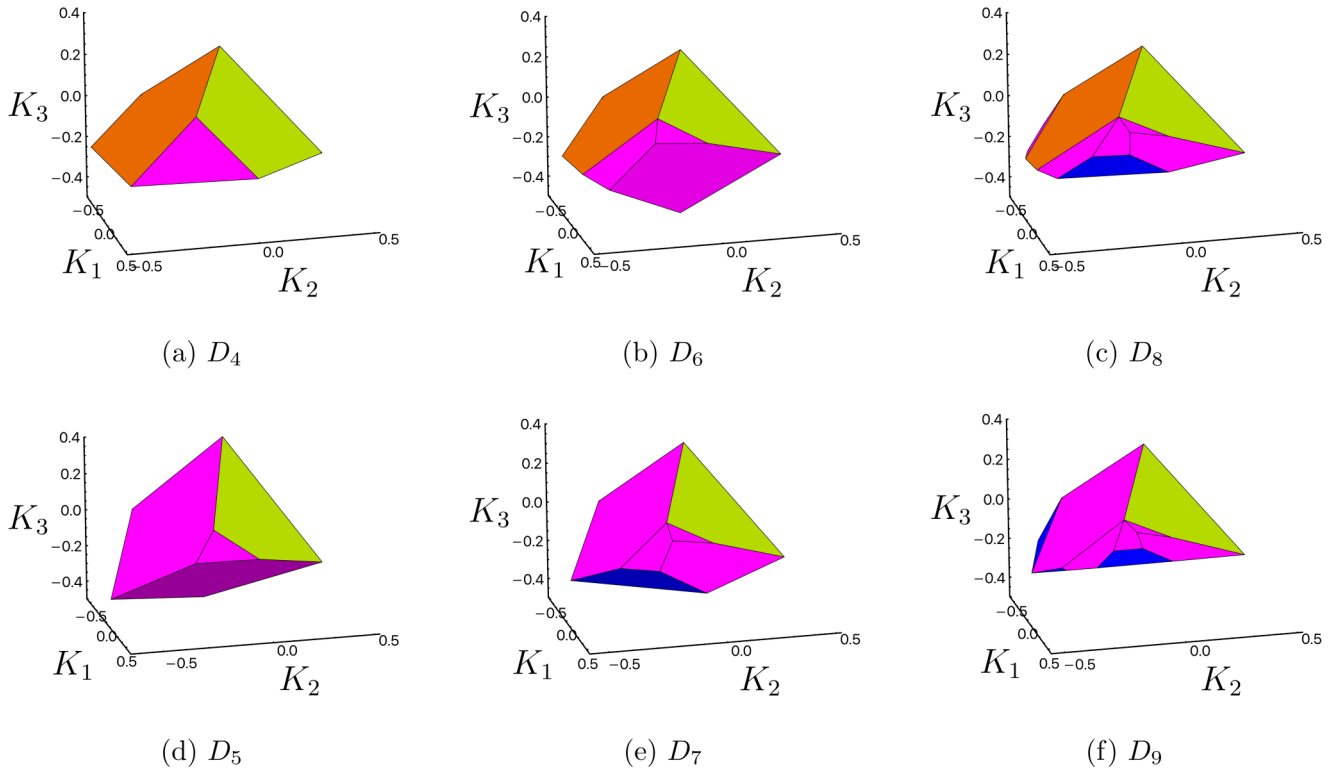

(a) D_4 (b) D_6 (c) D_8

(d) D_5 (e) D_7 (f) D_9

FIG. 6. The disorder polytopes D_4 through D_9. Faces are color coded for the multiplicity M of the associated unstable mode: $M = 1$: green; $M = 2$: brown; $M = 4$: purple; $M = 8$: blue.

disorder polytope is examined in more detail in Appendix D 2. An important result is the identification of the topmost vertex $\mathbf{K}^T = (0, 0, 1/4)$ of D_N in the limit $N \to \infty$. We also notice that as N increases, the difference between the successive even and odd polytopes appears to decrease. As we will explicitly show later on, this difference indeed disappears in the limit.

Next, in Figs. 7(a)–7(d), we show the even polytopes from $N = 10$ to $N = 16$. Again a number of features stand out. As N increases, the complexity of the bottom of the polytope in the half space $K_3 < 0$, where as we argued the system is strongly frustrated, increases. Moreover, we see a marked clustering of the faces corresponding to modes with multiplicity $M = 4$ into *fan*-like structures, while those belonging to modes with multiplicity $M = 8$ seem to string out along a curve, which we will call the *ridge*. These structures are brought into focus in Figs. 7(e) and 7(f), where we show a view of D_{16} and D_{32} "from below" with a viewpoint on the negative K_3 axis. The detailed analysis of the fan modes in Appendix D 3 identifies the apices of these structures in the limit $N \to \infty$ as $\mathbf{K}^S = (1/2, -1/4, 0)$, $\mathbf{K}^{MS} = (-1/2, -1/4, 0)$, and $\mathbf{K}^{DS} = (0, 1/2, -1/4)$ for the fans associated with stripe, modulated stripe, and diagonal stripe modes, respectively. The analysis of the ridge in Appendix D 4 yields the explicit form of the ridge in the limit $N \to \infty$ as

$$\mathbf{K}^R(a) = \frac{1}{4\cos(2\pi a) + \cos(4\pi a) + 5}\left[4\,\mathrm{sign}(1/2 - a)\cos^2(\pi a), -1, -\frac{1}{2}\right], \quad a \in [0, 1], \tag{26}$$

with its lowest point labeled as $\mathbf{K}^B = \mathbf{K}^R(1/2) = (0, -1/2, -1/4)$.

TABLE I. Number of faces of the disorder polytopes as function N compared to $|\hat{\mathfrak{U}}_N|$.

N	4	5	6	7	8	9	10	12	14	16
Faces	6	6	10	10	14	15	20	26	34	42
$\lvert\hat{\mathfrak{U}}_N\rvert$	6	6	10	10	15	15	21	28	36	45

Finally, in Table I, we list the number of faces of the disorder surface as a function N compared to the maximal number of modes available, which indicates that for even N, a number of modes does not contribute a face to D_N. In Appendix D 5, we characterize these *faceless* modes.

B. The limit $N \to \infty$

1. The natural coordinate frame

As $\mathbf{F}$ is a vector-valued mapping from the two-dimensional domain $\widehat{\mathfrak{U}}_\infty$ to $\mathbb{R}^3$, it is clear that there must be a dependency

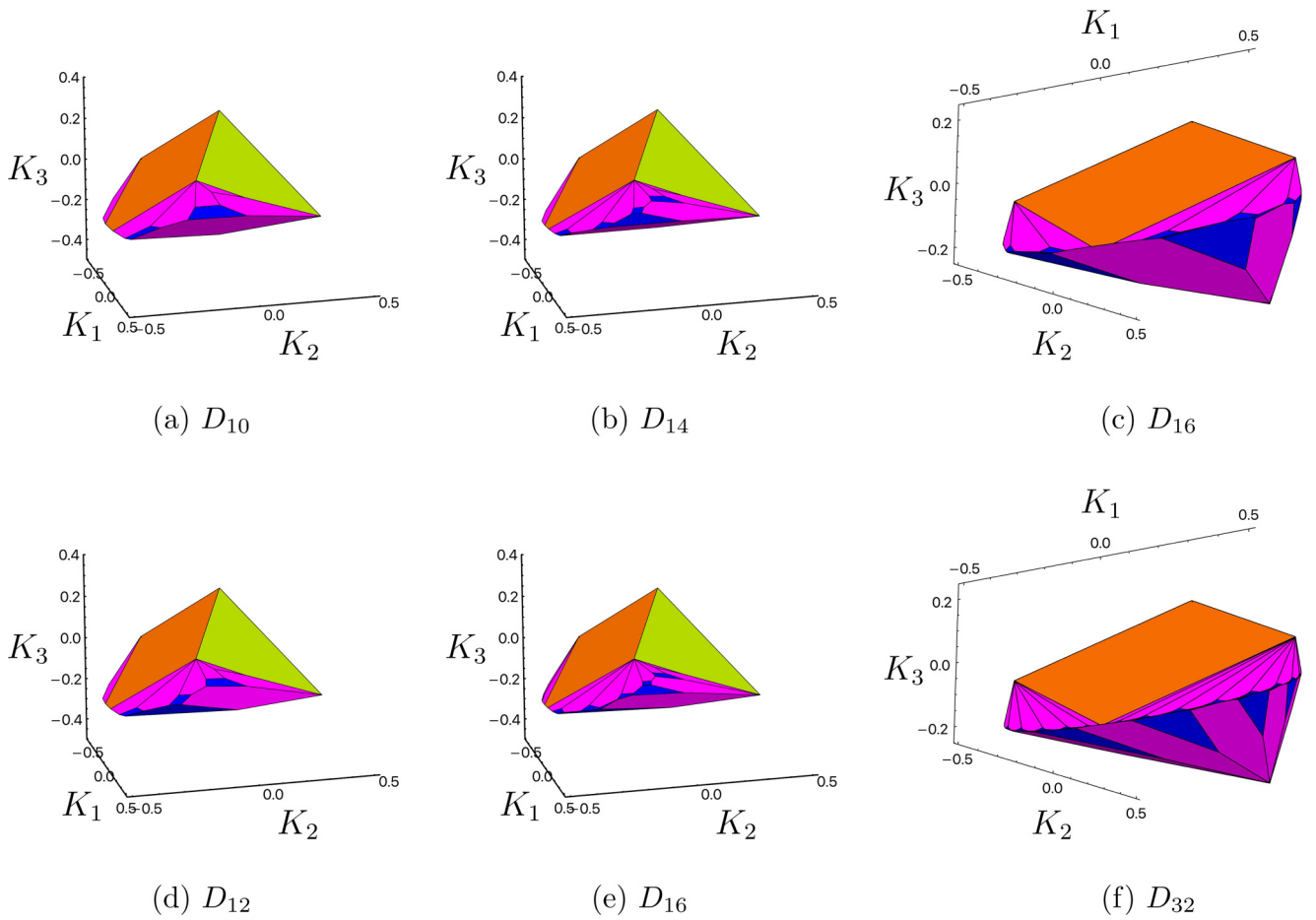

FIG. 7. The even disorder polytopes D_{10} through D_{16} and the "bottom" view of D_{16} and D_{32}. Faces are color coded for the multiplicity M of the associated unstable mode: $M = 1$: green; $M = 2$: brown; $M = 4$: purple; $M = 8$: blue. D_{16} and D_{32} further show the fans of striped, modulated stripe, and diagonal stripe $M = 4$ modes (purple) emanating from the vertices $\mathbf{K}^S$, $\mathbf{K}^{MS}$, and $\mathbf{K}^{DS}$, respectively, as well as the $M = 8$ modes (blue) that cluster around the so-called ridge. Note the decrease in area of the wedgelike $M = 8$ modes that interdigitate the diagonal stripe fan as N increases.

between the elements of $\mathbf{F}(\mathfrak{q})$. Indeed, we find that

$$\begin{aligned} F_1(\mathfrak{q})^2 &= (2\cos q_1 + 2\cos q_2)^2 \\ &= 2[2\cos(q_1 - q_2) + 2\cos(q_1 + q_2)] \\ &\quad + 2\cos 2q_1 + 2\cos 2q_2 + 4 \\ &= 2F_2(\mathfrak{q}) + F_3(\mathfrak{q}) + 4. \end{aligned} \tag{27}$$

This allow us to define a new coordinate frame with orthonormal basis vectors $\hat{\mathbf{n}}_1 = (1, 0, 0)$, $\hat{\mathbf{n}}_2 = (0, 1/\sqrt{5}, -2/\sqrt{5})$, and $\hat{\mathbf{n}}_3 = (0, 2/\sqrt{5}, 1/\sqrt{5})$, which represents a clockwise rotation of the original frame by an angle $\chi = \arctan 2$ around the K_1 axis. Defining the coordinates with respect to this frame through $\varphi_j = \mathbf{F}(\mathfrak{q}) \cdot \hat{\mathbf{n}}_j$, we find that $\varphi_3 = \frac{1}{\sqrt{5}}(\varphi_1^2 - 4)$, so that we are left with the simple representation

$$\mathbf{F}(\varphi_1, \varphi_2) = \varphi_1 \hat{\mathbf{n}}_1 + \varphi_2 \hat{\mathbf{n}}_2 + \frac{1}{\sqrt{5}}\big(\varphi_1^2 - 4\big)\hat{\mathbf{n}}_3. \tag{28}$$

The details of this transformation, as well as the shape of the IBZ in the new coordinates, are presented in Appendix E.

2. Surface reconstruction

We now ask, given the relatively simple parametrization given by Eq. (28), whether it is possible to reconstruct D_∞ from the definition $\mathbf{F}(\varphi_1, \varphi_2) \cdot \mathbf{K}(\varphi_1, \varphi_2) = 1$, the relation that characterizes the boundary points; cf. Eq. (14). To that end, we introduce $\hat{\mathbf{u}}(\varphi_1, \varphi_2) = \mathbf{F}(\varphi_1, \varphi_2)/|\mathbf{F}(\varphi_1, \varphi_2)|$ and note that this is the unit normal to the surface $\mathbf{K}(\varphi_1, \varphi_2)$. The defining equation then reads

$$\hat{\mathbf{u}}(\varphi_1, \varphi_2) \cdot \mathbf{K}(\varphi_1, \varphi_2) = \frac{1}{|\mathbf{F}(\varphi_1, \varphi_2)|} \equiv h(\varphi_1, \varphi_2), \tag{29}$$

which introduces the *support function* h. It is a standard result of convexity theory (see, e.g., [33]) that a convex body is fully determined by its support function. As the domain of our parametrization of the body is a compact set with only piecewise smooth boundary, we will need to perform the necessary inversion in the interior, the smooth boundary components, and the extreme points separately.

Interior: The ridge.. For notational brevity, we omit the explicit dependence of all dependent variables on the coordinates φ_j, and denote the partial derivatives $\partial/\partial\varphi_j$ simply by

∂_j. The vectors $\partial_i \mathbf{K}$ are, by definition, tangent to the surface, so we have that

$$\partial_i(\hat{\mathbf{u}} \cdot \mathbf{K}) = \partial_i \hat{\mathbf{u}} \cdot \mathbf{K} + \hat{\mathbf{u}} \cdot \partial_i \mathbf{K} = (\partial_i \hat{\mathbf{u}}) \cdot \mathbf{K} = \partial_i h. \quad (30)$$

Also, as $\hat{\mathbf{u}} \cdot \hat{\mathbf{u}} = 1$, we have $\partial_i \hat{\mathbf{u}} \cdot \hat{\mathbf{u}} = 0$, so that $\partial_i \hat{\mathbf{u}}$ are also vectors in the tangent plane. This implies that

$$\mathbf{K} = h\hat{\mathbf{u}} + \gamma_1 \partial_1 \hat{\mathbf{u}} + \gamma_2 \partial_2 \hat{\mathbf{u}}. \quad (31)$$

To obtain the unknown coefficient functions γ_i, we consider

$$(\partial_1 \hat{\mathbf{u}}) \cdot \mathbf{K} = \gamma_1 \partial_1 \hat{\mathbf{u}} \cdot \partial_1 \hat{\mathbf{u}} + \gamma_2 \partial_1 \hat{\mathbf{u}} \cdot \partial_2 \hat{\mathbf{u}} = \partial_1 h, \quad (32)$$

$$(\partial_2 \hat{\mathbf{u}}) \cdot \mathbf{K} = \gamma_1 \partial_2 \hat{\mathbf{u}} \cdot \partial_1 \hat{\mathbf{u}} + \gamma_2 \partial_2 \hat{\mathbf{u}} \cdot \partial_2 \hat{\mathbf{u}} = \partial_2 h, \quad (33)$$

which is readily solved by

$$\begin{pmatrix} \gamma_1 \\ \gamma_2 \end{pmatrix} = \frac{1}{\Delta(\hat{\mathbf{u}})} \begin{pmatrix} \partial_2 \hat{\mathbf{u}} \cdot \partial_2 \hat{\mathbf{u}} & -\partial_1 \hat{\mathbf{u}} \cdot \partial_2 \hat{\mathbf{u}} \\ -\partial_2 \hat{\mathbf{u}} \cdot \partial_1 \hat{\mathbf{u}} & \partial_1 \hat{\mathbf{u}} \cdot \partial_1 \hat{\mathbf{u}} \end{pmatrix} \begin{pmatrix} \partial_1 h \\ \partial_2 h \end{pmatrix}, \quad (34)$$

where the determinant is given by $\Delta(\hat{\mathbf{u}}) = (\partial_1 \hat{\mathbf{u}} \cdot \partial_1 \hat{\mathbf{u}})(\partial_2 \hat{\mathbf{u}} \cdot \partial_2 \hat{\mathbf{u}}) - (\partial_1 \hat{\mathbf{u}} \cdot \partial_2 \hat{\mathbf{u}})^2$. The explicit calculation is performed using *Mathematica* and yields the curve

$$\mathbf{K}^R(\varphi_1) = \frac{2\varphi_1}{4+\varphi_1^2}\hat{\mathbf{n}}_1 - \frac{\sqrt{5}}{4+\varphi_1^2}\hat{\mathbf{n}}_3. \quad (35)$$

This result implies that for fixed φ_1, the mode instability surfaces with different values of φ_2 are all tangent to a single ridgelike structure. Substituting $\varphi_1 = \mathrm{sign}(\varphi_1)\, 4\cos^2(a\pi)$ and transforming back to the original frame then shows that this is, in fact, the ridge given by Eq. (26) as calculated in a limit procedure in Appendix D 4. This proves the perhaps surprising fact that as we already hypothesized on the basis of the finite-N results, *all* the $M = 8$ modes that make up the interior of the IBZ become unstable on a set of measure zero in phase space.

The boundary: The fans.. Referring to Fig. 10 and Eqs. (E4) and (E5), we see that for each φ_1, there are two limiting tangent planes whose orientations are determined by $\mathbf{F}(\varphi_1, \varphi_2^{\max}(\varphi_1))$ and $\mathbf{F}(\varphi_1, \varphi_2^{\min}(\varphi_1))$, respectively. The former corresponds to a diagonal stripe mode, whereas the latter corresponds to striped ($\varphi_1 > 0$) and modulated stripe ($\varphi_1 < 0$) modes. Thus, from each location on the ridge, there are two straight lines with given orientation that end up in the already identified apices of the fans, i.e., the points $\mathbf{K}^S$, $\mathbf{K}^{MS}$, and $\mathbf{K}^{DS}$. Hence, in this limit, the fans become sectors of a generalized cone with, as base, (a segment of) the ridge. These cone sectors are ruled surfaces, which we can conveniently parametrize as

$$\mathbf{K}^X(\varphi_1, l) = \mathbf{K}^R(\varphi_1) + l[\mathbf{K}^X - \mathbf{K}^R(\varphi_1)], \quad l \in [0,1], \quad (36)$$

where X labels the specific apical vertex of the cone sector.

The extreme points: The major modes.. The three extreme points of the IBZ simply yield the major modes already discussed in Sec. IV B that dominate the phase diagram for $K_3 > 0$ already for finite N. It is now straightforward to verify that the faces of the major modes meet the fans along a set of four straight edges, $\mathbf{K}^S - \mathbf{K}^{DS}$, $\mathbf{K}^S - \mathbf{K}^B$, $\mathbf{K}^{MS} - \mathbf{K}^{DS}$, and $\mathbf{K}^{MS} - \mathbf{K}^B$.

TABLE II. The components of the surface of the order-disorder surface ∂D_∞. Here, conv($\mathbf{K}_1, \mathbf{K}_2, \ldots$) denotes the convex hull of the set of points in the argument list. The free parameters a and l take on values on the interval [0, 1].

Type	Symbol	Mode(s)	M	Specification
Major modes	F	(0,0)	1	conv($\mathbf{K}^T, \mathbf{K}^S, \mathbf{K}^{DS}$)
	AF	(π, π)	1	conv($\mathbf{K}^T, \mathbf{K}^{MS}, \mathbf{K}^{DS}$)
	AS	$(\pi, 0)$	2	conv($\mathbf{K}^T, \mathbf{K}^S, \mathbf{K}^{MS}, \mathbf{K}^B$)
Fans	S	$(a\pi, 0)$	4	$\mathbf{K}^R(\varphi_1) + l[\mathbf{K}^S - \mathbf{K}^R(\varphi_1)]$
	MS	$(\pi, a\pi)$	4	$\mathbf{K}^R(\varphi_1) + l[\mathbf{K}^{MS} - \mathbf{K}^R(\varphi_1)]$
	DS	$(a\pi, a\pi)$	4	$\mathbf{K}^R(\varphi_1) + l[\mathbf{K}^{DS} - \mathbf{K}^R(\varphi_1)]$
Ridge	R	all others	8	$\mathbf{K}^R(\varphi_1)$ $\varphi_1 \in [-4, 4]$

3. *The geometry of D_∞ and its implications*

With all these components in place, we can now give the full description of D_∞ analytically, by enumerating the components of its boundary ∂D_∞ in Table II, and visually, in Fig. 8.

Two features immediately stand out. First, roughly half of the surface area of the order-disorder surface is formed by the three planar facets associated with the major modes $\mathfrak{q}^F$ and $\mathfrak{q}^{AF}$, the two front-facing triangles, and $\mathfrak{q}^{AS}$, the back-facing quadrilateral. These three modes represent the simplest possible magnetization patterns consistent with the lattice structure, being either homogeneous or, at most, of period 2 in any direction. The flatness of the faces implies that the corresponding states can be robustly selected by choosing a suitable set of coupling constants. Let $\mathbf{K} \equiv \kappa \hat{\mathbf{K}}$, with $|\hat{\mathbf{K}}| = 1$ a unit vector in coupling space and κ the corresponding inverse temperature variable. Consider choosing $\hat{\mathbf{K}}$ such that there is a κ^* so that $\kappa^* \hat{\mathbf{K}}$ lies in one of these faces, and hence locates the transition from the disordered state to a state with order described by the corresponding major mode. Clearly, by continuity, it is always possible to choose a neighboring unit vector $\hat{\mathbf{K}}'$ such that the

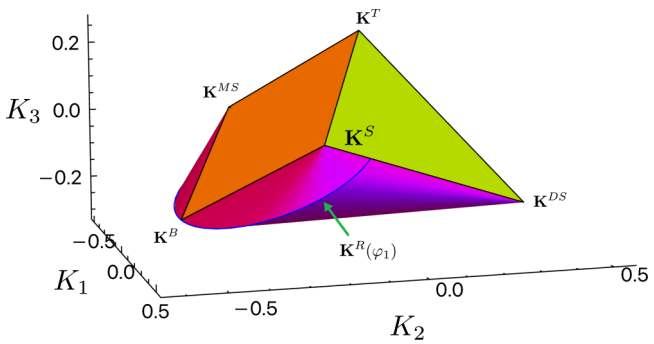

FIG. 8. The disordered region D_∞. The top region consist of three facets corresponding to transitions towards the ferromagnetic phase (front), the antiferromagnetic phase (hidden behind), and the alternating striped phase (back). The bottom region consists of three generalized cones, shown with a shading that highlights their curvature, with apices at the vertices $\mathbf{K}^S$, $\mathbf{K}^{MS}$, and $\mathbf{K}^{DS}$, which are the locus of transitions characterized by the (quasi)-one-dimensional $M = 4$ unstable modes. These cones are separated by the ridge $\mathbf{K}^R(\varphi_1)$ [see Eq. (35)], which is the locus of the more complex $M = 8$ unstable modes.

ray $\kappa\hat{\mathbf{K}}'$ also intersects the same face, and hence also leads to a transition into the same state.

Second, the remaining part of the surface area, which in its entirety lies in the region $K_3 < 0$ where frustration effects are dominant, is curved. Apart from a set of measure zero, i.e., the ridge, this area corresponds to transitions to states with ordering governed by the three one-parameter families of (quasi)-one-dimensional modes with multiplicity $M = 4$. By construction, a specific mode selected remains constant on any straight line connecting one of the fan apices $\mathbf{K}^S$, $\mathbf{K}^{MS}$, and $\mathbf{K}^{DS}$ to the ridge. However, when moving away from any point on the surface corresponding to a critical mode in any direction not along one of these "rules" of the surface, one inevitably probes the curvature and traverses points at which there is a transition to other neighboring modes. Specifically, consider $\mathfrak{q}(\lambda) = \lambda(\pi, 0), (\pi, \lambda\pi)$, or $\lambda(\pi, \pi)$, with $\lambda \in (0, 1)$, i.e., an interior point of one of the three edges of the IBZ. Now choose a set of coupling constants $\mathbf{K}^* = \kappa^*\hat{\mathbf{K}}$ such that $\mathbf{K}^* \cdot \mathbf{F}(\mathfrak{q}(\lambda)) = 1$ and hence marks the location of the transition to the state with dominant mode $\mathfrak{q}(\lambda)$. By continuity, we now have that there are neighboring sets of coupling constants $\hat{\mathbf{K}}'$ whose ray $\kappa\hat{\mathbf{K}}'$ will intersect the order-disorder surface at a point marking the transition to a mode $\mathfrak{q}(\lambda')$, where λ' is any arbitrary point in the neighborhood of λ. As the rationals are dense in the reals, this means that by perturbing the coupling constants, the system can undergo a transition to states with dominant modes of arbitrary finite wavelength, but also, in case λ' is irrational, to essentially random aperiodic structures. This implies that the part of the phase diagram beyond what we could perhaps aptly call this "devil's surface" is irreducibly complex, consisting of a dense array of measure zero sheet-like domains, with the dominant unstable mode changing in complexity essentially arbitrarily as one moves from sheet to sheet.

VI. COMPARISON WITH SIMULATIONS

It is clearly infeasible to test the predicted devil's-surface-like complexity of the mode structure of the nascent phases at parts of the order-disorder boundary by numerical means. However, our analysis of finite periodicities with fixed index N, which led to the definition of the disorder polytopes D_N, showed that these are all realized on the common $N \times N$ square periodicity. The latter condition is readily realized by imposing periodic boundary conditions in a standard single spin-flip Metropolis simulation. This allows us to assess how including fluctuations up to a certain wavelength impacts the predictions of the mean-field approximations, in which these fluctuations are, by definition, neglected.

To be able to limit ourselves to a finite number of simulations, we make the following choice. For fixed N, we consider the set of bifurcating modes $\{\mathfrak{q}_f\}$, where f indexes the set of faces of D_N. For each mode $\mathfrak{q}_f$, we determine a representative coupling vector $\mathbf{K}^*_f$ as the centroid of the face it belongs to. We then perform a series of simulations along the ray in phase space, $\beta\mathbf{K}^*_f$, $\beta \in [0, \infty)$. The scaled inverse temperature β is thus chosen so that the predicted transition occurs at $\beta = 1$, which allows for easy comparison with the simulations independent of the details of each face.

In order to analyze the results of the simulation, we need a suitable order parameter to signal the presence (or nonpresence) of certain modes. As we will perform multiple replicates of the simulations at each inverse temperature, this order parameter has to be insensitive to any of the possible global symmetries that link different replicates. Defining the Fourier transform of the site magnetization pattern by

$$\hat{m}_{\mathfrak{q}} = \frac{1}{N} \sum_{z \in \mathcal{U}_{\mathrm{P}}} m_z e^{-i\langle \mathfrak{q}, z\rangle}, \tag{37}$$

we can define

$$\mu_{\mathfrak{q}} \equiv \frac{1}{|\mathfrak{D}_4|} \sum_{g \in \mathfrak{D}_4} \hat{m}^*_{g\mathfrak{q}} \hat{m}_{g\mathfrak{q}}. \tag{38}$$

By virtue of being square in the magnetizations, this expression divides out the up-down symmetry of the Hamiltonian. By multiplying complex conjugates, the translation symmetries, which generate unitary phase factors, are divided out. Finally, the explicit "averaging" over the point group symmetries divides out the remaining symmetries.

We performed simulations for $N = 4, 6, 8, 12$. As a proof of principle, we show the order parameter values for the emergent modes beyond each of the 10 faces of D_6 in Fig. 9. The results for the other N values were similar (data not shown).

For ease of reference, these plots are organized to mimic the geometry of the salient IBZ, $\widehat{\mathfrak{U}}_6$. In all cases, the observed dominant mode is the one predicted by our mean-field analysis. Moreover, in all cases, the other modes, which have fairly significant amplitudes due to inevitable finite-size effects in the disordered phase, appear to be suppressed in the ordered regime. Strikingly, the shape of the order parameter curves also obeys the predicted symmetry in the antidiagonal of the IBZ (see Appendix D 1). Finally, and as expected, the mean-field analysis appears to underestimate the value of the inverse temperature at which the ordering transition occurs. In Appendix F, we provide a few more technical details about the simulations.

VII. DISCUSSION

Our analysis of the order-disorder transitions of the field-free NNNN Ising model on the square lattice shows that the observation by Landau and Binder, in their seminal paper on this topic almost four decades ago [8], that "Using mean-field theory, we also find indications of interesting behavior for $T > 0$," was prescient. Our results indicate that in this approximation, the strong frustration induced by antiferromagnetic NNNN interactions produces fully developed complexity already at the level of the high-temperature order-disorder transition. Indeed, a large part of the order-disorder surface in the half space $K_3 < 0$ represents a devil's surface, where bifurcating modes of arbitrary complexity are densely interspersed.

Our results also bring to the fore a hitherto perhaps less appreciated role for the lattice symmetry group and its action on the space of lattice modes by showing that the multiplicity M of these modes under the point group is a strong determinant of whether and where in the phase space these modes become unstable. Strikingly, the $K_3 > 0$ part of the order-disorder surface is entirely determined by the three major modes at the extreme points of the IBZ, while the three one-parameter families of $M = 4$ modes associated with the edges of the IBZ, all located in the half space $K_3 < 0$, make up the remaining

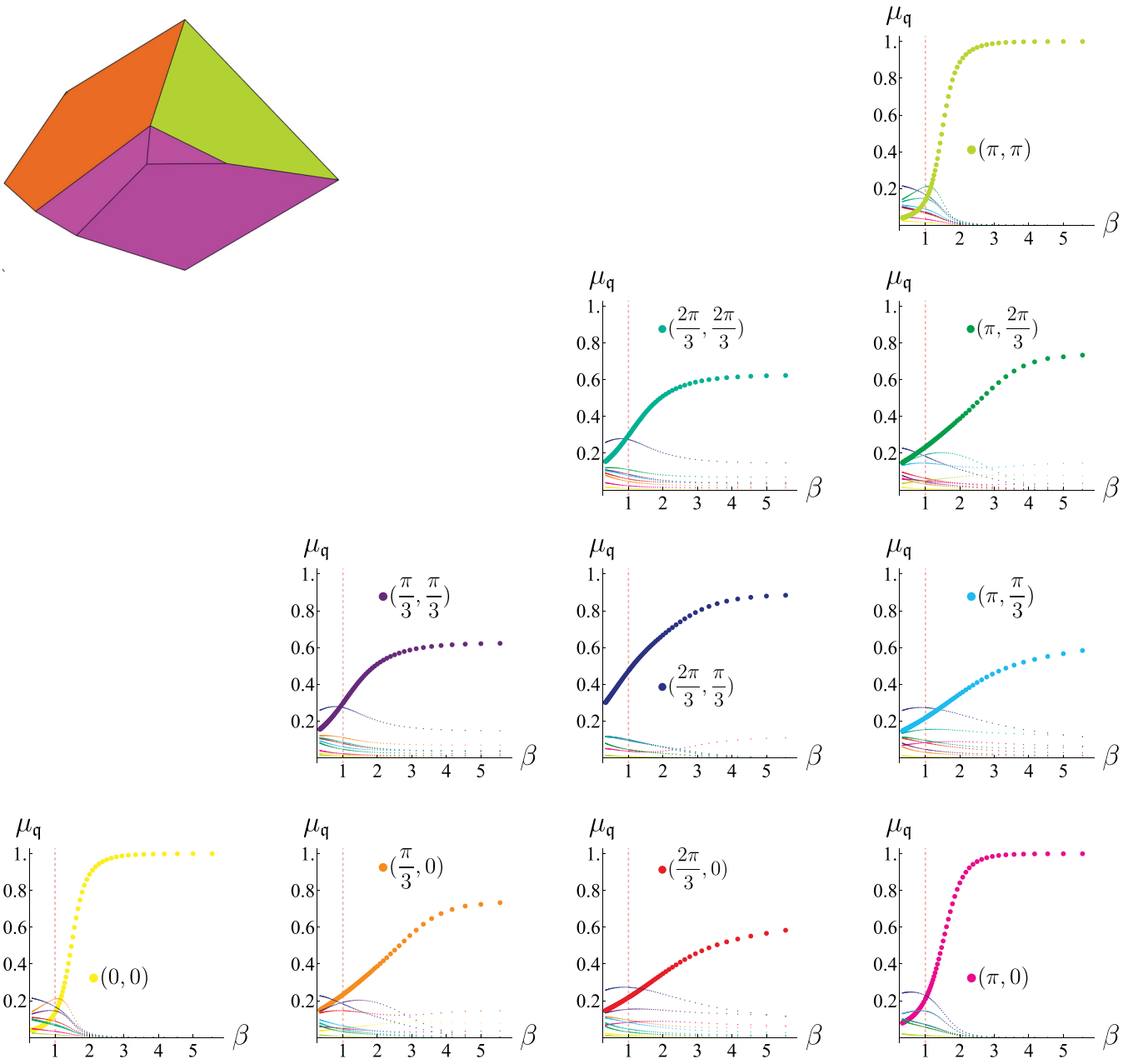

FIG. 9. Order parameter μ_q as function of the reduced inverse temperature β for all possible modes on a 6×6 periodic lattice, for coupling constants corresponding to the centroid of each of the 10 possible faces of D_6, here visualized in the upper left corner. In all cases, the predicted bifurcating mode is the sole dominant one.

surface area. Thus a set of measure zero in the IBZ accounts for all the bifurcation modes, except for a set of measure zero, i.e., the ridge, to which all the $M = 8$ modes, which represent the full measure of the IBZ, are compressed. It is our intuition that these results can possibly be interpreted within the setting of the so-called equivariant branching lemma [34,35], a cornerstone of the theory of bifurcations with symmetry, which identifies a role for solutions with "maximal" residual symmetry with respect to the symmetry group being broken.

All together, these results provide a somewhat paradoxical answer to our original question of the designability of complex patterns in binary lattice gases. On the one hand, the antiferromagnetic NNNN interactions enable a vast array of patterns to become accessible directly from the disordered phase. On the other hand, the ultrasensitive dependence on the precise values of the coupling constants, implied by the devil's surface for the $M = 4$ modes and the collapse onto a set of zero measure of the $M = 8$ modes, effectively precludes a requisite degree of control in selecting specific patterns. It is an interesting question whether it is possible to circumvent the latter defect, perhaps through multispin interactions, and construct a system with a more robust, yet sufficiently rich, phase behavior.

Obviously, the mean-field approach is a serious approximation, and one may well ask whether any of these features survives the inclusion of the inevitably strong correlations

in a low-dimensional system such as the 2D square lattice. Here, we were able to provide limited evidence using Monte Carlo simulations that at least some of the predictions remain valid when we include these correlations up to cutoff imposed by periodic boundary conditions. Specifically, we correctly predict the dominant mode developing from the disordered phase along rays in phase space that pass through the center of the faces of the calculated disorder polytopes D_N. The "optimistic" view suggests that we can expect that results on the nature of symmetry-breaking events, which are, to a large extent, constrained by purely group-theoretical properties, may be more universal, and hence transcend the specific approximation chosen.

There are several directions of further research suggested by our results. First, it would be interesting to study this system beyond the mean-field approximation, perhaps using a variant of the cluster variation method [36]. Obvious questions are as follows: (i) does the order-disorder surface remain a convex polytope and, (ii) if so, which of its features remain invariant. Next, one could explore the immediate generalizations of the bifurcation conditions given by Eq. (12) to different lattices and/or longer-range interactions. The analysis framework we set up here can readily be extended in these directions, albeit that as we increase the interaction range, we also increase the dimensionality of the disorder polytopes with a concomitant increase of geometrical complexity. So far, we have also limited our analysis to the order-disorder surface. What happens beyond it is an open question. We have indications that at least for finite N, the dimensionality of the solution spaces associated with the bifurcating modes is significantly smaller than N, which would possibly make it tractable to at least numerically track these solutions to possible lower-temperature transitions. We certainly expect that secondary transitions are likely to occur, as most of the bifurcating modes only partially break the symmetry of the underlying lattice. Although we did not dwell on this here, our simulations also point to the occurrence of such transitions.

It would also be interesting to see what, if anything, the present analysis reveals about the ground-state phase diagram. Here, the recently developed method of mapping the ground-state problem of arbitrary spin models into a maximum-satisfiability problem [37], or other recent approaches to the ground-state problem in frustrated systems such as tensor network analysis [38] or the so-called cluster tree optimization algorithm [39], may prove useful.

Finally, on a much more abstract level, there recently has been a series of papers that focuses on the universality and complexity of classical spin models from the perspective of the theory of computation [40–42]. It would be fascinating to explore what these insights could contribute to understanding the present system and frustrated systems in general.

ACKNOWLEDGMENTS

The authors would like to thank David Avis and Charles "Skip" Jordan for their kind assistance in using lrs. This work is part of the Dutch Research Council (NWO) and was performed at the research institute AMOLF.

APPENDIX A: PERIODIC PATTERNS ON $\mathbb{Z}^2$

A magnetization *pattern* $m(\mathrm{z})$ is periodic if there exist two basis vectors $\mathrm{p}_1 = (p_1^1, p_1^2)$, $\mathrm{p}_2 = (p_2^1, p_2^2) \in \mathbb{Z}^2$ such that

$$\forall k_1, k_2 \in \mathbb{Z} : m(\mathrm{z}+k_1\mathrm{p}_1 + k_2\mathrm{p}_2) = m(\mathrm{z}). \tag{A1}$$

It is convenient to parametrize the periodicity through the matrix

$$\mathrm{P} = \begin{pmatrix} p_1^1 & p_1^2 \\ p_2^1 & p_2^2 \end{pmatrix}, \tag{A2}$$

where, without loss of generality and by convention, we choose the order of the basis vectors such that the *index* of the periodicity $\det(\mathrm{P}) = N \equiv p_1^1 p_2^2 - p_1^2 p_2^1 > 0$. The unit cell associated with this pattern is then defined as

$$\mathcal{U}_\mathrm{P} = \left\{ \mathrm{z} \in \mathbb{Z}^2 \middle| \begin{array}{l} 0 \leqslant \langle \mathrm{z}, \mathrm{p}_1\rangle\langle \mathrm{p}_2, \mathrm{p}_2\rangle - \langle \mathrm{z}, \mathrm{p}_2\rangle\langle \mathrm{p}_1, \mathrm{p}_2\rangle < N^2, \\ 0 \leqslant \langle \mathrm{z}, \mathrm{p}_2\rangle\langle \mathrm{p}_1, \mathrm{p}_1\rangle - \langle \mathrm{z}, \mathrm{p}_1\rangle\langle \mathrm{p}_1, \mathrm{p}_2\rangle < N^2 \end{array} \right\}. \tag{A3}$$

Note that the number of lattice points in the unit cell is given by the index $|\mathcal{U}| = N$. The set $\widehat{\mathcal{U}}_\mathrm{P}$ of wave vectors compatible with this periodicity must satisfy

$$\langle \mathrm{q}, \mathrm{p}_1\rangle = 2\pi k_1, \tag{A4}$$

$$\langle \mathrm{q}, \mathrm{p}_2\rangle = 2\pi k_2, \tag{A5}$$

for some $\mathrm{k} = (k_1, k_2) \in \mathbb{Z}^2$, so that $\exp(i\,\langle \mathrm{q}, \mathrm{z}+l_1\mathrm{p}_1 + l_2\mathrm{p}_2\rangle) = \exp(i\,\langle \mathrm{q}, \mathrm{z}\rangle)$ for all $l_1, l_2 \in \mathbb{Z}$. Writing (A4) and (A5) as

$$\mathrm{Pq} = 2\pi\mathrm{k}, \tag{A6}$$

we have

$$\mathrm{q} = 2\pi\mathrm{P}^{-1}\mathrm{k}. \tag{A7}$$

We now introduce the dual basis $\hat{\mathrm{p}}_1 = (p_1^1, p_2^1)$ and $\hat{\mathrm{p}}_2 = (p_1^2, p_2^2)$, and note that $\mathrm{P}^{-1}\hat{\mathrm{p}}_1 = \mathrm{e}_1$ and $\mathrm{P}^{-1}\hat{\mathrm{p}}_2 = \mathrm{e}_2$. Thus, $\mathrm{q}' = 2\pi\mathrm{P}^{-1}(\mathrm{k} + l_1\hat{\mathrm{p}}_1 + l_2\hat{\mathrm{p}}_2) = \mathrm{q} + 2\pi l_1\mathrm{e}_1 + 2\pi l_2\mathrm{e}_2$, and hence $\mathrm{Pq}' = 2\pi\mathrm{k} + 2\pi l_1\mathrm{Pe}_1 + 2\pi l_2\mathrm{Pe}_2 \equiv 2\pi\mathrm{k}'$. So, adding integer multiples of the dual basis vectors to k does not yield additional information, and we can restrict ourselves to solutions in the dual unit cell (discrete Brillouin zone),

$$\widehat{\mathcal{U}}_\mathrm{P} = \left\{ \mathrm{q} = 2\pi\mathrm{P}^{-1}\mathrm{k} \middle| \mathrm{k} \in \mathbb{Z}^2, \begin{array}{l} 0 \leqslant \langle \mathrm{k}, \hat{\mathrm{p}}_1\rangle\langle \hat{\mathrm{p}}_2, \hat{\mathrm{p}}_2\rangle - \langle \mathrm{k}, \hat{\mathrm{p}}_2\rangle\langle \hat{\mathrm{p}}_1, \hat{\mathrm{p}}_2\rangle < N^2 \\ 0 \leqslant \langle \mathrm{k}, \hat{\mathrm{p}}_2\rangle\langle \hat{\mathrm{p}}_1, \hat{\mathrm{p}}_1\rangle - \langle \mathrm{k}, \hat{\mathrm{p}}_1\rangle\langle \hat{\mathrm{p}}_1, \hat{\mathrm{p}}_2\rangle < N^2 \end{array} \right\}, \tag{A8}$$

where we have used that $\det(\mathrm{P}^T) = \det(\mathrm{P}) = N$, which also shows that there are $|\widehat{\mathcal{U}}_\mathrm{P}| = |\mathcal{U}_\mathrm{P}| = N$ independent wave vectors that are compatible with the periodicity.

In the following, we would like to enumerate all possible periodicities, classifying them according to their index N. This problem is equivalent to enumerating all the subgroups of

$\mathbb{Z}^2$ of index N. This can be performed employing a theorem due to Hermite [43], which states that for any matrix with integer entries $\mathrm{P} \in GL_2(\mathbb{Z})$ and determinant N, there is a unimodular (determinant-preserving up to sign) transformation $\mathrm{J} \in GL_2(\mathbb{Z})$, such that $\mathrm{P}^* = \mathrm{PJ}$, where P^* is of the form

$$\mathrm{P}^* = \begin{pmatrix} d_1 & 0 \\ 0 \leqslant s_1 < d_1 & d_2 = \frac{N}{d_1} \end{pmatrix}, \tag{A9}$$

the so-called lower-triangular Hermite normal form. These matrices thus fall into equivalence classes, which are enumerated by considering that for any divisor $d_1|N$, there are exactly d_1 inequivalent forms, and hence $|\{\mathrm{P}|\det \mathrm{P} = N\}| = \sum_{d_1|N} d_1 \equiv \sigma_1(N)$. This implies that one can simply choose as the basis of our desired pattern the vectors $\mathrm{p}_1^* = (d_1, 0)$ and $\mathrm{p}_2^* = (0 \leqslant s_1 < d_1, d_2 = N/d_1)$. Note, however, that these vectors need not be the set of minimal length basis vectors that generate the same periodic sublattice. If necessary, these so-called Minkowski bases can be obtained from the Hermite normal form basis, through an algorithm due to Lagrange [44].

Next, we introduce

$$\widehat{\mathcal{U}}_N = \bigcup_{\{\mathrm{P}||\widehat{\mathcal{U}}_\mathrm{P}|=N\}} \widehat{\mathcal{U}}_\mathrm{P}, \tag{A10}$$

i.e., the set of all lattice wave vectors compatible with periodic patterns with index N. We can now prove the following, as far as we can tell, nontrivial lemma:

Lemma 1. $\widehat{\mathcal{U}}_N = \{\mathrm{q} = \frac{2\pi}{N}(l_1, l_2) | 0 \leqslant l_1, l_2 < N\}$ and hence $|\widehat{\mathcal{U}}_N| = N^2$.

We prove this lemma in two steps. First, consider the periodicity Π, with basis vectors $\pi_1 = (N, 0)$ and $\pi_2 = (0, N)$, i.e., a square $N \times N$ unit cell. We have $\mathcal{U}_\Pi = \{\mathrm{z}|0 \leqslant z^1, z^2 < N\}$. Also, $\widehat{\mathcal{U}}_\Pi = \frac{2\pi}{N}\mathcal{U}_\Pi$. Let the periodicity P with index N be given by the basis vectors $\mathrm{p}_1 = (d, 0)$ and $\mathrm{p}_2 = (s, \bar{d})$, where $d \in [N]$ (the set of divisors of N) and the complementary divisor is defined as $\bar{d} \equiv N/d$. Now, $\pi_1 = \bar{d}\mathrm{p}_1$ and $\pi_2 = -s\mathrm{p}_1 + d\mathrm{p}_2$. It follows that any P periodic pattern is also Π periodic, and hence $\widehat{\mathcal{U}}_\mathrm{P} \subset \widehat{\mathcal{U}}_\Pi$ and

$$\widehat{\mathcal{U}}_N = \bigcup_{\{\mathrm{P}|\widehat{\mathcal{U}}_\mathrm{P}|=N\}} \widehat{\mathcal{U}}_\mathrm{P} \subset \widehat{\mathcal{U}}_\Pi. \tag{A11}$$

We then need to prove the reverse inclusion by showing that for every $\mathrm{q} = \frac{2\pi}{N}(l_1, l_2)$, there is a P with $\det \mathrm{P} = N$ such that $\mathrm{q} \in \widehat{\mathcal{U}}_\mathrm{P}$. Recall that $\mathrm{P}^{-1}\hat{\mathrm{p}}_1 = \mathrm{e}_1$ and $\mathrm{P}^{-1}\hat{\mathrm{p}}_2 = \mathrm{e}_2$, so that $\mathrm{k} = \frac{l_1}{N}\hat{\mathrm{p}}_1 + \frac{l_2}{N}\hat{\mathrm{p}}_1$ would be a valid solution provided $\mathrm{k} \in \mathbb{Z}^2$. In the Hermite normal form representation, $\hat{\mathrm{p}}_1 = (d, s)$ and $\hat{\mathrm{p}}_2 = (0, \bar{d})$. Thus the question reduces to whether $d \in [N]$ and $0 \leqslant s < d$ can be chosen such that the congruences

$$l_1 d \equiv 0 \mod N, \tag{A12}$$

$$l_1 s + l_2 \bar{d} \equiv 0 \mod N \tag{A13}$$

hold. We distinguish two cases:

(i) l_1 does *not* divide N ($l_1 \nmid N$): In this case, congruence (A12) can only be solved by taking $d = N$. This reduces the second one to $l_1 s \equiv N - l_2 \mod N$. In this case, $m \equiv \mathrm{GCD}(l_1, N) = 1$ and hence $m \mid N - l_2$, guaranteeing a solution [45].

(ii) l_1 divides N ($l_1 \mid N$): In this case, $l_1 = d_1$ with $d_1 \in [N]$, but $d_1 \neq N$, so that (A12) is solved by $d = \bar{d}_1$, and the second condition reduces to $d_1 s + l_2 d_1 \equiv 0 \mod N$, which in turn reduces to $s + l_2 \equiv 0 \mod \bar{d}_1$. Let $l_2 = n\bar{d}_1 + r_2$; then the latter congruence is trivially solved by $s = \bar{d}_1 - r_2$.

This shows that

$$\widehat{\mathcal{U}}_\Pi \subset \widehat{\mathcal{U}}_\mathrm{P} \subset \widehat{\mathcal{U}}_N \tag{A14}$$

and, hence, $\widehat{\mathcal{U}}_\Pi = \widehat{\mathcal{U}}_N$.

APPENDIX B: THE SIZE OF THE SETS $\widehat{\mathfrak{U}}_N$

Now, let $s_M(N)$ count the numbers of orbits with multiplicity M in $\widehat{\mathfrak{U}}_N$. The only two modes which have an orbit of length $M = 1$ are (0,0) and (π, π), and hence $s_1(N) = 1$ for N odd and $s_1(N) = 2$ for N even. $(0, \pi)$ is the only mode with orbit length $M = 2$; accordingly, $s_2(N) = 1$ for N even and zero otherwise. For the remaining two cases, it is convenient to define $N_s = \lfloor \frac{N-1}{2} \rfloor$ for N odd and $N_s = \lfloor \frac{N-2}{2} \rfloor$ for N even. The number of modes with orbit length $M = 4$ is given by $s_4(N) = 3N_s$ for N even and $s_4(N) = 2N_s$ for N odd. The orbits of length $M = 8$ are, independently of the parity of N, given by $s_8(N) = \sum_{n=1}^{N_s} n = \frac{1}{2}N_s(N_s + 1)$. Thus, the size of $\widehat{\mathfrak{U}}_N$ is simply given by

$$\begin{aligned} |\widehat{\mathfrak{U}}_N| &= s_1(N) + s_2(N) + s_4(N) + s_8(N) \\ &= \frac{1}{2}\left\lfloor \frac{N+2}{2} \right\rfloor \left(\left\lfloor \frac{N+2}{2} \right\rfloor + 1 \right). \end{aligned} \tag{B1}$$

This is equivalent to the more intuitive formula

$$|\widehat{\mathfrak{U}}_N| = \sum_{n=1}^{\lfloor \frac{N}{2}+1 \rfloor} n, \tag{B2}$$

which can also be understood geometrically by referring to Fig. 3. Note that this analysis also correctly reproduces the size of $\widehat{\mathcal{U}}_N$,

$$|\widehat{\mathcal{U}}_N| = s_1(N) + 2s_2(N) + 4s_4(N) + 8s_8(N) = N^2. \tag{B3}$$

APPENDIX C: THE VERTEX ENUMERATION ALGORITHM

The coefficients of the inequalities given by Eq. (20) defining the half spaces that bound the disorder polytopes are generically irrational by virtue of the definition of $\mathbf{F}(\mathrm{q})$ [Eqs. (16)–(18)]. However, the vertex enumeration algorithm lrs that we employed intrinsically uses exact integer arithmetic. Thus we are forced to rationalize the components $\mathbf{F}(q)$ as input to the program. As a consequence of this approximation, some artifacts are to be expected, primarily in the form of spurious vertices. We empirically observed, e.g., that the resulting polytopes output by lrs are all *simple*, i.e., all of their vertices have degree 3, where the *degree* of a vertex is the number of edges, and hence also the number of faces, to which it belongs. The analysis presented in Appendix D 3 below, however, shows that the vertices at the apex of the so-called fan modes $\mathbf{K}^S$, $\mathbf{K}^{MS}$, and $\mathbf{K}^{DS}$ are *degenerate* as their degree in fact diverges in the limit $N \to \infty$.

We have identified three sources of spurious vertices and developed appropriate corrective procedures for all of them.

First, as already alluded to above, the vast majority of the spurious vertices appear around the apices of the fans, which we know analytically and hence readily detected and removed. In fact, if a fan apex has degree k, we find that exactly $k-1$ spurious vertices are generated, which are much closer among each other than the typical distance $d \sim 0.1$ to the nearest distinct vertex. The second category of spurious vertices is associated with the faceless modes (Appendix D 5) that are all tangent to a common edge. We empirically found that each faceless mode contributed exactly two spurious vertices in the neighborhood of the common edge, which we subsequently removed. The final category is composed of spurious vertices that are "accidental" and only occur for the interior $M=8$ modes. They occur when components of $\mathbf{F}(q)$ for neighboring q's happen to be identical, but because of finite precision arithmetic are mapped to different rational approximations. These then have to be dealt with through explicit analytical recalculation. In practice, we never observed more than four such spurious vertices for all N's considered (up to $N=256$). Defining the degree of rationalization Δ as the number of digits allowed for numerator and/or denominator in the approximants, we found that it is a useful rule of thumb to suspect all pairs vertices closer than Δ^{-3} as being spurious.

APPENDIX D: FEATURES OF THE FINITE-N DISORDER POLYTOPE

1. Odd-even effects

On the square lattice, we can define a unique parity of each site by defining $\|\mathrm{z}\| = (z_1 + z_2) \mod 2$. Considering Fig. 1, we see that the standard neighborhood set N_1 consists of sites with parity 1, while both N_2 and N_3 only contain sites with parity 0. This implies that for every solution m_z of the bifurcation equation (12) with coupling constants $\mathbf{K} = (K_1, K_2, K_3)$, there is a solution $\bar{m}_z = (-)^{\|z\|} m_z$ with coupling constants $\bar{\mathbf{K}} = (-K_1, K_2, K_3)$. Fourier transforming $\bar{m}_z$, we find that $\bar{\mathrm{q}} = \mathrm{q} - (\pi, \pi)$. We also find that $F_1(\bar{\mathrm{q}}) = -F_1(\mathrm{q})$, while $F_2(\bar{\mathrm{q}}) = F_2(\mathrm{q})$ and $F_3(\bar{\mathrm{q}}) = F_3(\mathrm{q})$, so that if $\mathbf{K}\cdot\mathbf{F}(\mathrm{q}) = 1$, then $\bar{\mathbf{K}}\cdot\mathbf{F}(\bar{\mathrm{q}}) = 1$ and therefore also solves Eq. (14). Referring to Fig. 2, we see that the mapping $\mathrm{q} \to \mathrm{q} - (\pi, \pi)$ corresponds to the reflection r with respect to what we call the *antidiagonal*, the perpendicular bisector onto the hypotenuse of the symmetry-reduced Brillouin zone $\widehat{\mathfrak{U}}_\infty$. We now ask under what conditions $\mathfrak{q} \in \widehat{\mathfrak{U}}_N \Rightarrow r\mathfrak{q} \in \widehat{\mathfrak{U}}_N$. As $\mathfrak{q} = (2\pi\frac{i}{N}, 2\pi\frac{j}{N})$, $0 \leqslant j \leqslant i \leqslant \lfloor \frac{N}{2} \rfloor$, we have $r\mathfrak{q} = (\frac{N-2j}{N}\pi, \frac{N-2i}{N}\pi)$, so that $r\mathfrak{q} \in \widehat{\mathfrak{U}}_N$ if and only if N is even, as is also illustrated in Fig. 3. Thus, any facet of D_{2N} associated with mode $\mathfrak{q}$ and normal vector $\mathbf{F}(\mathfrak{q})$ is paired with a facet with mode $\bar{\mathfrak{q}}$ and normal vector $\mathbf{F}(\mathfrak{q}) = \mathbf{F}(r\mathfrak{q})$, and the whole polytope is mirror symmetric with respect to the plane $K_1 = 0$ for all even N.

2. The major modes

The three faces that bound the polytope in the half space $K_3 > 0$ are associated with the modes that are located at the extreme points of the IBZ $\widehat{\mathfrak{U}}_N$. Defining

$$q_N^m = \left\lfloor \frac{N}{2} \right\rfloor \frac{2\pi}{N}, \tag{D1}$$

these are the modes $\mathfrak{q}_0 = (0,0)$, $\mathfrak{q}_1 = (q_N^m, 0)$, and $\mathfrak{q}_2 = (q_N^m, q_N^m)$. As $q_{2k}^m = \pi$, these facets are the same for all even N. In that case, it is easy to see they represent the *ferromagnetic* ($\mathfrak{q}^F$), *alternating striped* ($\mathfrak{q}^{AS}$), and *antiferromagnetic* ($\mathfrak{q}^{AF}$) ordering patterns, respectively. These modes are visualized in Fig. 4. Also, as $q_{2k+1}^m = \pi\frac{2k}{2k+1}$, we see $\lim_{k\to\infty} q_{2k+1}^m = \pi$, so that as N increases, the odd top facets converge to the even ones. A direct computation of the location of the top vertex $\mathbf{K}^T$ of the polytope, obtained by solving the conditions $\mathbf{K}\cdot\mathbf{F}(\mathfrak{q}^F) = \mathbf{K}\cdot\mathbf{F}(\mathfrak{q}^{AS}) = \mathbf{K}\cdot\mathbf{F}(\mathfrak{q}^{AF}) = 1$, then yields, for even N, the vertex $\mathbf{K}^T = (0, 0, \frac{1}{4})$, while for odd $N = 2k+1$, we have $\mathbf{K}_{odd}^T = (\frac{1}{4}\{1 + 1/[2\cos(\pi\frac{2k}{2k+1}) + 1]\}, 0, -1/[8\cos(\pi\frac{2k}{2k+1}) + 4])$. The latter, as expected, converges to $\mathbf{K}^T$ as $k \to \infty$.

3. The edge modes and the fans

The three fans of faces shown most clearly in Figs. 7(e) and 7(f) are associated with the multiplicity $M=4$ modes on the edges of the IBZ. We distinguish the modes of the form $\mathfrak{q}^S(i) = (2\pi i/N, 0)$, $i = 1, \ldots, l(N)$, on the horizontal leg, which are associated with *striped* ordering patterns, modes of the form $\mathfrak{q}^{MS}(i) = (\pi, 2\pi i/N)$, $i = 1, l(N)$ on the vertical leg, which we associate with *modulated-stripe* ordering patterns, and the modes on the hypotenuse of the form $\mathfrak{q}^{DS}(i) = (2\pi i/N, 2\pi i/N)$, $k = 1, \ldots, l(N)$, which we associate with *diagonal stripe* ordering patterns, where $l(2k) = k-1$ and $l(2k+1) = k$. These modes are visualized in Fig. 4.

We can show by explicit construction that the facets corresponding to any three successive fan modes share a common vertex, which moreover is independent of which triplet is considered. For the striped modes, we find, on solving $\mathbf{K}\cdot\mathbf{F}(\mathfrak{q}^S(i-1)) = \mathbf{K}\cdot\mathbf{F}(\mathfrak{q}^S(i)) = \mathbf{K}\cdot\mathbf{F}(\mathfrak{q}^S(i+1)) = 1$, the vertex $\mathbf{K}^S = (1/2, -1/4, 0)$ for all N. The analogous calculation for the modulated-stripe modes yields, for even N, the vertex $\mathbf{K}^{MS} = (-1/2, -1/4, 0)$, consistent with the symmetry of D_{2k} discussed above, while for odd $N = 2k+1$, we find $\mathbf{K}_{odd}^{MS} = \{\frac{1}{2}\sec(\frac{2\pi k}{2k+1}), -\frac{1}{4}\sec^2(\frac{2\pi k}{2k+1}), 0\}$, which converges to $\mathbf{K}^{MS}$ for $k \to \infty$. Finally, for the diagonal stripe modes, we find $\mathbf{K}^{DS} = (0, 1/2, -1/4)$ for all N. Details of how these fans meet in the middle area of the bottom of the polytopes will be addressed in the following section.

4. The interior modes and the ridge

The interior modes with multiplicity $M=8$ have fewer remaining symmetries. A few examples are shown in Fig. 4. As Figs. 7(e) and 7(f) suggest, the faces corresponding to these modes are directly connected to the striped and modulated stripe fans and are clustered around an increasingly narrow quasi-one-dimensional structure which we call the ridge. This structure can be characterized by considering the common vertex belonging to the faces corresponding to two successive modes along either of the legs of the IBZ and one of the interior $M=8$ modes nearest to this pair. Considering, e.g., the pair striped modes $[\mathfrak{q}^S(i), \mathfrak{q}^S(i+1)]$ on the horizontal leg, the nearest interior mode is $\mathfrak{q}^{int}(i) = (2\pi i/N, 2\pi/N)$, and we solve for $\mathbf{K}\cdot\mathbf{F}(\mathfrak{q}^S(i)) = \mathbf{K}\cdot\mathbf{F}(\mathfrak{q}^S(i+1)) = \mathbf{K}\cdot\mathbf{F}(\mathfrak{q}^{int}(i)) = 1$. For finite N, the resulting analytical expressions for the solution $\mathbf{K}^{ridge}(i)$ are rather unwieldy and

we refrain from presenting them. However, by parametrizing $i = aN,\ a \in [0, 1/2]$, we can take the limit $N \to \infty$, yielding

$$\mathbf{K}^R(a) = \frac{1}{4\cos(2\pi a) + \cos(4\pi a) + 5}\left[4\cos^2(\pi a), -1, -\frac{1}{2}\right]. \tag{D2}$$

A similar analysis for the modulated-stripe modes on the vertical leg, now parameterized by $i = (1/2 - a)N,\ a \in [0, 1/2]$, yields, as expected by the reflection symmetry in the antidiagonal of the IBZ, the same result mirrored in the plane $K_1 = 0$. We also note that the ridge is a planar curve embedded in the plane $K_2 = 2K_3$. For future reference, we name the two end points of the ridge $\mathbf{K}^R_\pm = (\pm 2/5, -1/10, -1/20)$ and the lowest point on the curve $\mathbf{K}^B \equiv \mathbf{K}^R(1/2) = (0, -1/2, -1/4)$.

One also notices that the faces belonging to the diagonal stripe fan are "split" by wedge-shaped faces belonging to $M = 8$ modes. The vertices at which this happens can be found by considering the common vertex between two subsequent diagonal stripe modes $[\mathfrak{q}^{DS}(i), \mathfrak{q}^{DS}(i+1)]$ with their common nearest interior mode $[2\pi(i+1)/N, 2\pi i/N]$. Using a similar parametrization as above, i.e., $i = bN,\ b \in [0, 1/2]$, and passing to the limit $N \to \infty$, we obtain the curve

$$\mathbf{K}^W(b) = \left(\frac{\cos(2\pi b)}{\cos(4\pi b) + 2}, 0, -\frac{1}{4(\cos(4\pi b) + 2)}\right). \tag{D3}$$

However, by considering the angle between the pair of edges defined by the two pair of modes $(\mathfrak{q}^{DS}(i), [2\pi(i+1)/N, 2\pi i/N])$ and $([2\pi(i+1)/N, 2\pi i/N], \mathfrak{q}^{DS}(i+1))$, one can show that the surface area of these wedgelike $M = 8$ faces vanishes in the limit $N \to \infty$.

5. The faceless modes

The so-called faceless modes for even N are all located on the *antidiagonal* that runs from the vertex $\mathfrak{q}^{AF} = (\pi, 0)$ to the midpoint of the hypotenuse of the IBZ. These modes can generically be parameterized as $\mathfrak{q}^{AD}(\alpha) = (\pi - \alpha, \alpha),\ \alpha \in [0, \pi/2]$. It follows that $\mathbf{F}(\mathfrak{q}^{AD}(\alpha)) = [0, -2(1 + \cos 2\alpha), 4\cos 2\alpha]$. Considering the family of planes defined through $\mathbf{K} \cdot \mathbf{F}[\mathfrak{q}^{AD}(\alpha)] = 1$, we see that these share a common line of intersection given by $(K_1, -1/2, -1/4)$. Hence only the planes defined by the relevant endpoints, $\mathfrak{q}^{AS} = (\pi, 0)$ and $\mathfrak{q}^{AD} = (\pi/2, \pi/2)$ for $N = 4k$ or $\mathfrak{q}^{AD} = [2\pi(k+1)/(4k+2), 2\pi k/(4k+2)]$ for $N = 4k + 2$ (see Fig. 3) can contribute a face to D_N, and all the modes between these endpoints do not, which exactly explains the pattern observed in Table I. We note, however, that these modes will of course play a role for $\mathbf{K}$ values located on the common edge they share.

APPENDIX E: THE NATURAL COORDINATE SYSTEM

Slightly rewriting Eq. (27), we have $F_1(\mathfrak{q})^2 - 4 = 2F_2(\mathfrak{q}) + F_3(\mathfrak{q})$, which suggests a new basis vector along (0,2,1). Trivially, a vector along $(0, 1, -2)$ is then orthogonal to both the latter and the invariant axis along (1,0,0). Normalizing these vectors yields the frame $\hat{\mathbf{n}}_j$ given in the main text. The explicit form of the two independent coordinates is

$$\varphi_1 = 2\cos q_1 + 2\cos q_2 \equiv 2\xi_1 + 2\xi_2, \tag{E1}$$

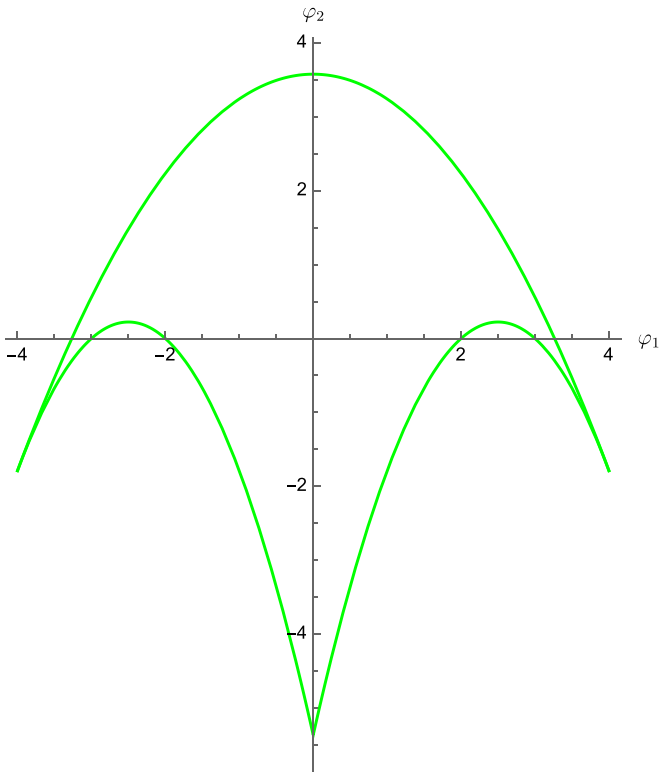

FIG. 10. The shape of $\widehat{\Phi}_\infty$, the image of the IBZ $\widehat{\mathfrak{U}}_\infty$ expressed in the natural coordinates φ_j.

$$\begin{aligned}\varphi_2 &= \frac{2}{\sqrt{5}}[\cos(q_1 - q_2) + \cos(q_1 + q_2) - 2\cos 2q_1 \\ &\quad -2\cos 2q_2] \\ &= \frac{4}{\sqrt{5}}\left(2 + \cos q_1 \cos q_2 - 2\cos^2 q_1 - 2\cos^2 q_2\right) \\ &\equiv \frac{4}{\sqrt{5}}\left(2 + \xi_1\xi_2 - 2\xi_1^2 - 2\xi_2^2\right),\end{aligned} \tag{E2}$$

where we have introduced $\xi_1 = \cos q_1$ and $\xi_2 = \cos q_2$. The mapping $(q_1, q_2) \to (\xi_1, \xi_2)$ maps $\widehat{\mathfrak{U}}_\infty$ to $\widehat{\Xi}_\infty = \{(\xi_1, \xi_2) | -1 \leqslant \xi_1 \leqslant \xi_2 \leqslant 1\}$. Clearly, on this domain $\varphi_1 \in [-4, 4]$. Eliminating ξ_2 then yields

$$\varphi_2 = -2\frac{10\xi_1^2 - 5\xi_1\varphi_1 + \varphi_1^2 - 4}{\sqrt{5}}. \tag{E3}$$

For a given φ_1, we need to ensure that $(\xi_1, \xi_2) \in \Xi_\infty$, which yields the constraint $\xi_1 \in [\max(-1, \frac{1}{2}\varphi_1 - 1), \frac{1}{4}\varphi_1]$. This yields the two limiting curves

$$\varphi_2^{\max}(\varphi_1) = \frac{2}{\sqrt{5}}\left(4 - \frac{3}{8}\varphi_1^2\right), \tag{E4}$$

$$\varphi_2^{\min}(\varphi_1) = -\frac{2}{\sqrt{5}}(2 - |\varphi_1|)(3 - |\varphi_1|), \tag{E5}$$

where the first curve corresponds to the diagonal edge of $\widehat{\mathfrak{U}}_\infty$, and the lower curve to the horizontal leg when $\varphi_1 > 0$ and the vertical leg when $\varphi_1 < 0$. The three extreme points $\mathfrak{q}^F$, $\mathfrak{q}^{AF}$, and $\mathfrak{q}^{AS}$ are mapped to $\varphi^F = (4, -4/\sqrt{5})$, $\varphi^{AF} = (-4, -4/\sqrt{5})$, and $\varphi^{AS} = (0, -12/\sqrt{5})$, respectively. The do-

main of values $\widehat{\Phi}_\infty$ in the φ parametrization that corresponds to $\widehat{\mathfrak{U}}_\infty$ is shown in Fig. 10.

APPENDIX F: DETAILS OF THE SIMULATIONS

The Monte Carlo (MC) simulations were implemented in C++ and performed on a local computing cluster. Following the discussion in Sec. VI, we consider rays in phase space through the centroids of the predicted faces of D_N on $N \times N$ square lattices with $N = 4, 6, 8, 12$. The specific state points were chosen by sampling the inverse temperature $T = 1/\beta$ on 40 equally spaced points in the range $T \in [1, 3]$ and 45 points in the lower-temperature range. Finally, on the lattice of size $N = 12$, we refined the temperature resolution even further to $\Delta T = 0.01$ for $T < 0.5$.

To compute the average of observables and their standard deviations, we employed block averaging, using $n_B = 100$ blocks. In order to choose the appropriate block length to ensure independence of the block averages, we estimated the autocorrelation "time" τ in MC sweeps (one attempted flip per spin in the lattice) for a number of observables. For $N = 4$ and $N = 6$, we were able to establish that the correlation time of the order parameter of the dominant mode was systematically larger, yet of similar order of magnitude than that of any of the other modes, and moreover did not strongly depend on the specific face of D_N considered. For the larger lattice sizes, we therefore limited ourselves to measuring the correlation time for the standard ferromagnetic order parameter on the ray through the face associated with $\mathfrak{q}^F = (0, 0)$. For $T > 0.4$, we systematically measured $\tau < 100$ for all lattice sizes, allowing $n_b = 10^4$. For $T \leqslant 0.4$, the correlation time increases rapidly and we employed block sizes of $n_b = 10^5$–10^6, with the exact value optimized for the specific temperature and system size. Finally, we note that the computational bottleneck of our simulations is actually the calculation of the order parameters. Due to their extreme small size, these systems are intrinsically noisy and subject to, e.g., drift. These means that local magnetizations quickly average out. We therefore needed to resort to calculating the order parameter on the basis of instantaneous configurations, and subsequently average these, which requires a costly Fourier transform at every sweep.

[1] W. M. Jacobs, A. Reinhardt, and D. Frenkel, Proc. Natl. Acad. Sci. **112**, 6313 (2015).
[2] G. H. Wannier, Phys. Rev. **79**, 357 (1950).
[3] M. P. Nightingale, Phys. Lett. A **59**, 486 (1977).
[4] R. H. Swendsen and S. Krinsky, Phys. Rev. Lett. **43**, 177 (1979).
[5] J. Oitmaa, J. Phys. A: Math. Gen. **14**, 1159 (1981).
[6] K. Binder and D. P. Landau, Phys. Rev. B **21**, 1941 (1980).
[7] D. P. Landau, Phys. Rev. B **21**, 1285 (1980).
[8] D. P. Landau and K. Binder, Phys. Rev. B **31**, 5946 (1985).
[9] J. L. Morán-López, F. Aguilera-Granja, and J. M. Sanchez, Phys. Rev. B **48**, 3519 (1993).
[10] R. A. dos Anjos, J. Roberto Viana, and J. Ricardo de Sousa, Phys. Lett. A **372**, 1180 (2008).
[11] A. Kalz, A. Honecker, S. Fuchs, and T. Pruschke, Eur. Phys. J. B **65**, 533 (2008).
[12] A. Kalz, A. Honecker, and M. Moliner, Phys. Rev. B **84**, 174407 (2011).
[13] S. Jin, A. Sen, and A. W. Sandvik, Phys. Rev. Lett. **108**, 045702 (2012).
[14] S. Jin, A. Sen, W. Guo, and A. W. Sandvik, Phys. Rev. B **87**, 144406 (2013).
[15] W. Selke, Phys. Rep. **170**, 213 (1988).
[16] S. H. Tindemans and B. M. Mulder, Phys. Rev. E **82**, 021404 (2010).
[17] J. Kanamori and M. Kaburagi, J. Phys. Soc. Jpn. **52**, 4184 (1983).
[18] U. Brandt, Z. Phys. B: Condens. Matter **53**, 283 (1983).
[19] F. A. Kassan-Ogly, A. K. Murtazaev, A. K. Zhuravlev, M. K. Ramazanov, and A. I. Proshkin, J. Magn. Magn. Mater. **384**, 247 (2015).
[20] R. M. Liu, W. Z. Zhuo, S. Dong, X. B. Lu, X. S. Gao, M. H. Qin, and J. M. Liu, Phys. Rev. E **93**, 032114 (2016).
[21] J. K. Glasbrenner, I. I. Mazin, H. O. Jeschke, P. J. Hirschfeld, R. M. Fernandes, and R. Valentí, Nat. Phys. **11**, 953 (2015).
[22] J. Kanamori, Prog. Theor. Phys. **35**, 16 (1966).
[23] N. Boccara, *Broken Symmetry: Theory of Transitions with Order Parameter* (Hermann, Paris, 1976).
[24] J. C. Tolédano and P. Tolédano, *The Landau Theory of Phase Transitions*, World Scientific Lecture Notes in Physics, Vol. 3 (World Scientific, Singapore, 1987).
[25] D. S. Dummit and R. M. Foote, *Abstract Algebra*, 3rd ed. (Wiley, New York, 2004).
[26] Note that any mode $\mathfrak{q}$ compatible with periodicity P is trivially also compatible with periodicity kP, $k \geqslant 2$.
[27] B. Grünbaum, in *Convex Polytopes*, edited by V. Kaibel, V. Klee, and G. M. Ziegler, Graduate Texts in Mathematics, Vol. 221 (Springer, New York, 2003).
[28] A. C. Reimers and L. Stougie, arXiv:1404.5584.
[29] D. Avis and C. Jordan, arXiv:1510.02545.
[30] D. Avis and K. Fukuda, Discrete Comput. Geom. **8**, 295 (1992).
[31] D. Avis and C. Jordan, Math. Program. Comput. **10**, 267 (2018).
[32] Wolfram Research, Inc., *Mathematica, Version 13.0.0* (Champaign, IL, 2021), https://www.wolfram.com/mathematica.
[33] R. Schneider, *Convex Bodies: The Brunn-Minkowski Theory* (Cambridge University Press, Cambridge, 2013).
[34] M. Golubitsky, I. Stewart, and D. G. Schaeffer, *Singularities and Groups in Bifurcation Theory*, Applied Mathematical Sciences, Vol. 69 (Springer, New York, 1988).
[35] M. Golubitsky and I. Stewart, *The Symmetry Perspective: From Equilibrium to Chaos in Phase Space and Physical Space* (Birkhäuser, Basel, 2003).
[36] A. Pelizzola, J. Phys. A: Math. Gen. **38**, R309 (2005).
[37] W. Huang, D. A. Kitchaev, S. T. Dacek, Z. Rong, A. Urban, S. Cao, C. Luo, and G. Ceder, Phys. Rev. B **94**, 134424 (2016).
[38] B. Vanhecke, J. Colbois, L. Vanderstraeten, F. Verstraete, and F. Mila, Phys. Rev. Res. **3**, 013041 (2021).
[39] W. Huang, D. Kitchaev, S. Dacek, Z. Rong, Z. Ding, and G. Ceder, arXiv:1606.07429.

[40] G. De Las Cuevas and T. S. Cubitt, Science **351**, 1180 (2016).
[41] T. Kohler and T. Cubitt, J. Stat. Phys. **176**, 228 (2019).
[42] D. Drexel and G. de las Cuevas, arXiv:2006.03529.
[43] C. Hermite, J. Reine Angew. Math. **1851**, 191 (1851).
[44] P. Q. Nguyen and D. Stehlé, Lect. Notes Comput. Sci. **3076**, 338 (2004).
[45] M. R. Schroeder, *Number Theory in Science and Communication*, Springer Series in Information Sciences, Vol. 7 (Springer, Berlin, 1997).